western australian marine science institution

Benthic community production and response to environmental forcing

Ryan J Lowe, Renee K Gruber, James L Falter

ARC Centre of Excellence for Coral Reef Studies, UWA Oceans Institute and School of Earth and Environment The University of Western Australia, Crawley, Western Australia, Australia

WAMSI Kimberley Marine Research Program

Final Report

Project 2.2.3

November 2016

western australian marine science institution

THE UNIVERSITY OF WESTERN AUSTRALIA

WAMSI Kimberley Marine Research Program

Initiated with the support of the State Government as part of the Kimberley Science and Conservation Strategy, the Kimberley Marine Research Program is co-invested by the WAMSI partners to provide regional understanding and baseline knowledge about the Kimberley marine environment. The program has been created in response to the extraordinary, unspoilt wilderness value of the Kimberley and increasing pressure for development in this region. The purpose is to provide science based information to support decision making in relation to the Kimberley marine park network, other conservation activities and future development proposals.

Front cover images (L-R)

Image 1: Satellite image of the Kimberley coastline

Image 2: Water cascading off Tallon reef crest during ebb tide (Source: Renee Gruber).

Image 3: Humpback whale breaching, Exmouth (Source: Pam Osborn)

Image 4: Azton Howard from Bardi Jawi Rangers filtering water sample for nutrient analysis (Source: Renee Gruber).

Year of publication: November 2016

Metadata: http://catalogue.aodn.org.au/geonetwork/srv/eng/metadata.show?uuid=d5b4b157-d0a1-48e3-a916-01aa8cecdf30

Citation: Lowe R, Gruber R, Falter J (2016) Benthic community production and response to environmental forcing. Report of Project 2.2.3 prepared for the Kimberley Marine Research Program, Western Australian Marine Science Institution, Perth, Western Australia, 43 pp.

Author Contributions: RL, RG and JF designed the field experiments, RL and RG conducted the field work and the data analysis, and RL, RG, and JF contributed to the report and wrote the related manuscripts.

Corresponding author and Institution: Ryan Lowe, The University of Western Australia, Ryan.Lowe@uwa.edu.au.

Funding Sources: This project was funded (commissioned) by the Western Australian Marine Science Institution as part of the WAMSI Kimberley Marine Research Program, a $30M program with seed funding of $12M provided by State government as part of the Kimberley Science and Conservation Strategy. The Program has been made possible through co-investment from the WAMSI Joint Venture partners. Additional funding was provided by Australian Research Council (ARC) Future Fellowship grant (FT110100201) to RJL.

Competing Interests: The commercial investors and data providers had no role in the data analysis, data interpretation, the decision to publish or in the preparation of manuscripts. The authors have declared that no competing interests exist.

Kimberley Traditional Owner agreement: This research was enabled by the Traditional Owners through their advice, participation and consent to access their traditional lands.

Acknowledgements: Our team would like to acknowledge the Bardi Jawi people, the Traditional Owners both past and present, who continue to care for this country. We thank the Bardi Jawi Rangers and staff of the Kimberley Marine Research Station for their skippering skills and help in the field. Mike Cuttler, Jordan Iles, Miela Kolomaznik, Leonardo Ruiz Montoya, and Nick Mortimer provided invaluable field assistance.

Collection permits/ethics approval: No collection occurred in the production of this report.

Contents

Executive Summary

Benthic primary producers such as corals, seagrasses and macroalgae, play significant roles in a variety of coastal processes. They provide habitat for numerous fauna, stabilise sediments, and form the basis of coastal food webs. Through photosynthesis, primary producers use sunlight as the energy source to transform dissolved carbon into new plant biomass. Tropical reef systems often display high rates of primary production; however, these rates are closely coupled to local physical (e.g., water motion, light, temperature) and biogeochemical (e.g., nutrient) environmental conditions. For example, previous studies have shown that high temperature and light levels can stress primary producers by negatively impacting photosynthesis. Our present understanding of environmental controls on reef productivity is based primarily on studies from the Caribbean, Hawaii, the southern Great Barrier Reef, and other Indo-Pacific regions, which contain mainly wave-dominated reefs. Tide-dominated reefs occur where the mean tidal range exceeds mean wave height, and constitute approximately 30% of tropical reefs worldwide. Tide-dominated reefs are known to experience much greater ranges in environmental conditions than wave-dominated reefs, yet the interactions between primary producers and environmental drivers that occur in these systems have been largely unstudied.

The goals of this project were to quantify the environmental variability across a macrotidal reef system in the Kimberley, and assess how benthic primary producers responded to extremes in water motion, light, and temperature. More specifically, we investigated: 1) how tides interacted with reef morphology to drive extreme daily variability in environmental conditions; 2) how this environmental variability influenced the productivity of benthic communities living in different zones of the reef platform; and 3) how water quality in coastal waters surrounding reefs varied over the wet/dry seasonal cycle.

To achieve these aims, we conducted three field experiments on an intertidal platform reef (Tallon Island) in the Sunday Island group of the west Kimberley. During each field experiment, we deployed an array of instruments measuring hydrodynamics, water temperature, light levels at the reef surface, and water column dissolved oxygen. Based on changes in water column oxygen, we were able to estimate community-scale (100s metres) rates of primary production in two distinct communities found on this reef: seagrass-dominated, and macroalgal-dominated (includes small corals and crustose coralline algae). Rates of primary production were then related to environmental data to assess whether communities were stressed during extremes in environmental conditions. In addition, we conducted intensive water quality sampling on the reef and in offshore channels to measure seasonal changes in dissolved and particulate nutrient concentrations and suspended chlorophyll.

Our findings show that macrotidal reefs in the Kimberley experience some of the most extreme conditions yet recorded for reefs worldwide. Extreme daily variability in temperature and dissolved oxygen occurs on the reef platform, and is driven by semi-diurnal tides and solar (light) cycles. The shape and friction of the platform causes water to 'pond' on the reef for up to 10 hours during each ebb tide (twice daily). When these extended low tide periods occur near noon, extreme warming happens on the reef, with temperatures rising by 10°C over several hours and reaching up to 38°C. This high light availability also drives high rates of benthic primary production, which releases oxygen into the water column and results in extremes in oxygen saturation (~270%). When low tide periods occur near midnight, community respiration (the consumption of oxygen and carbon to create energy) causes oxygen levels to plummet, reaching very low (hypoxic) levels; low oxygen levels are known to harm or kill organisms in other ecosystems, and are not typically recorded on reefs. We found that rates of gross primary production of the dominant communities (macroalgae and seagrass) were not adversely affected by environmental variability on this reef, emphasising the resilience of these organisms to extreme conditions. Productivity varied on a day-to-day basis, due to the timing of noon relative to low tide; this cycle lasts ~15 days, and future studies shorter than this time frame may over- or under-estimate ecological processes (such as productivity). Finally, the overall average rates of productivity we observed were similar to the global mean for tropical reefs, demonstrating that tide-dominated reefs can maintain moderate rates of production despite daily extremes in temperature.

Water quality (nutrient and chlorophyll levels) on the reef also displayed strong variability over tidal cycles, with particulate nutrients and phytoplankton (food sources for reef organisms) flooding the reef at high tide and being consumed during low tide. Towards the end of low tide, grazing depletes particles in the water column; thus, the tidal cycle is a key process that replenishes reef food sources. Our results also suggest that the seagrass zone may serve as an important nutrient subsidy to the macroalgal zone during low tides. Overall, Tallon reef was found to be oligotrophic (relatively low dissolved nutrients and chlorophyll), which is typical of tropical waters that do not receive substantial anthropogenic nutrient loads from terrestrial runoff. In waters surrounding the reef, increases in nutrient and chlorophyll concentrations occurred from the end of the dry season (Oct) through the wet season (Apr). Although significant, these differences are small, suggesting that waters at the mouth of King Sound are only mildly influenced by terrestrial inputs during low-rainfall wet seasons.

Implications for management

This study documents some of the many aspects of 'uniqueness' of Kimberley reefs, which experience conditions among the most extreme worldwide. Although our study was conducted on a single reef, intensive measurements of physical conditions (e.g., hydrodynamics, reef slope, reef morphology, and platform height above sea level) allow generalization of results to other Kimberley reefs. The Reef Geomorphology project (1.3.1) classified major Kimberley reefs and documented their morphology and height relative to sea level. These characteristics determine the length of low tide on a reef flat, and thus the extremes in environmental conditions such as water flow, temperature, light, dissolved oxygen, and pH that will develop there. Environmental extremes and productivity measured on other high intertidal reefs, such as Montgomery Reef and Irvine-Bathurst, would likely be very similar to those measured in our study of Tallon reef. Low intertidal reefs, such as Cockatoo Reef and other reefs growing well below sea level, would experience shorter low tide periods and thus a narrower range of environmental conditions. Sloping reef platforms would experience a much more subtle version of the 'ponding' effect on Tallon, with the extent of ebb tide elongation depending on the slope. Thus, physical relationships described in our study can help predict tidal patterns and environmental extremes on Kimberley reefs, provided some information on reef morphology is known.

Our results also provide a foundation for developing predictive models of conditions on Kimberley reefs under future climate change scenarios. As described above, temperature variability can be predicted on these reef platforms; this can be combined with predictions of ocean warming and sea level rise to estimate future conditions on reef platforms. For Tallon (and likely for similar reefs such as Montgomery), our estimates show that sea level rise may help mitigate mean ocean warming by damping temperature extremes on the platform. Such analyses could help prioritise management action or protection status in light of climate change predictions and other anthropogenic pressures.

Our results can also be used to help inform future monitoring exercises on Kimberley reefs, such as documenting high temperature events, or planning process-based scientific field studies. For high intertidal reefs (or where platform level is above mean sea level), the spring-neap cycle does not affect temperature or other conditions on the reef. Rather, the timing of noon relative to low tide is the primary driver of reef conditions. This cycle is ~15 days in length and is an important consideration for future studies focusing on any reef process affected by temperature, light, dissolved oxygen, etc. Studies less than ~15 days may greatly over- or under-estimate the process of interest. For low intertidal reefs (or where the platform is below mean sea level), the spring-neap cycle would be an additional driver of environmental variability. A high-frequency record of water depth at the study site is a key component of any future work, as it helps interpret results and position them within tidal and light cycles. In addition, although mean ocean temperature increased through the wet season, daily ranges of environmental conditions and reef productivity did not differ between seasons. This suggests that process-based studies during the wet season do not add any significant benefit over work during the dry season, when the Kimberley is far more accessible.

Finally, while we found that overall rates of productivity in this Kimberley reef system were comparable to

other coral reef habitats worldwide, the environmental conditions under which primary producers survive and grow are extreme. This has implications for the resilience of these producers in the face of climate change across the Kimberley environment. While these organisms appear well adapted to the local environmental conditions of the Kimberley, many are still likely operating at the edge of their capacity, as evidenced by coral bleaching in the inshore Kimberley associated with the El Niño heat wave in 2016 when temperatures across northern Australia were elevated for longer periods of time. Given the extreme conditions in temperature, oxygen levels and nutrients, management should consider strategies that will ensure any additional anthropogenic pressures that could add stress to the system are minimised and also be aware of environmental conditions that may change over time.

Key residual knowledge gaps

The project has provided a reasonably complete assessment of how environmental variability, including temperature, light, oxygen and water motion, influence the productivity of benthic reef communities in the Kimberley. Due to the process-focused nature of the experiments, we expect the general relationships and models developed in this project to be extended to other reef systems with some confidence. In other words, if the environmental conditions and benthic primary producers of other reefs are known, or can be reasonably predicted, we believe that robust estimates of the productivity of reefs across the Kimberley can be made.

Primary producers on Tallon's platform were highly tolerant to short-term extremes in temperature and light. This is likely due to the long time-scales (10s – 100s of years) over which communities have adapted to reef conditions. At present, it is unclear if this tolerance will convey resilience to any future ocean warming, both slow mean temperature increases and episodic warming events. Our results show that sea level rise will dampen temperature extremes on tide-dominated reefs. Will this mitigate ocean warming impacts on tide-dominated reefs in the long term? Additionally, our results suggest that low intertidal reefs are likely adapted to a more narrow range of environmental conditions. Will these reefs be more susceptible to the effects of ocean warming?

Our study was conducted during the 2013-2014 wet season, which experienced relatively low rainfall levels compared to the previous 20 years. While the results from this study indicated minor differences in reef water quality between seasons, this may not always be the case, particularly during more 'typical' wet years. Higher rainfall would likely result in nutrient and sediment pulses to coastal waters, driving phytoplankton production. Land-clearing and farming practices in coastal catchments increase these nutrient and sediment inputs, which has had a negative impact on reef health worldwide. At present, there is no data to assess whether changes planned for Kimberley catchments such as the Fitzroy River would substantially alter coastal water quality. Additionally, the Sunday Island group is relatively far (~100 km) from the closest major river (Fitzroy), but other reefs are much closer to river mouths, especially in the northern Kimberley. How does river discharge affect water quality surrounding those reefs? Knowledge of seasonal and spatial patterns in water quality would help better inform future management efforts of Kimberley reefs.

1 Introduction

Of all marine ecosystems, tropical reefs are among the most iconic and vibrant, and are generally considered to be among the most productive communities per area in the world (Crossland et al. 1991). Reefs provide many ecosystem services, including support of fisheries, coastal protection, and tourism (Moberg & Folke 1999). Unfortunately, many reefs have already experienced declines in health or are currently threatened by a host of anthropogenic activities (Bryant et al. 1998).

Early reef studies focused on "open ocean" systems in the Indo-Pacific region, which contained reefs that were oligotrophic, wave-dominated, and exposed to minimal terrestrial inputs. They had high coral cover, abundant light, and experienced low levels of environmental variability. Their morphology consisted of a steeply-sloping fore-reef, an energetic reef crest dominated by coralline algae, a reef flat dominated by a mosaic of coral, algae, and sand patches, and a sandy back-reef slope with scattered coral heads and outcrops (Odum & Odum 1955). Work over the past two decades has shown that productivity and nutrient uptake rates on reefs are related to mass transfer that controls how materials (e.g., nutrients, dissolved gasses, etc.) are exchanged between the water column and reef communities (a function of water velocity, bottom friction, solute concentration and diffusion characteristics) .

With only a few exceptions, most reef studies have found that the circulation of reefs is dominantly forced by either surface waves or tides, or a combination of the two (Monismith 2007, Falter et al. 2013, Lowe & Falter 2015). There are strong regional differences in the global distribution of significant wave heights (H_s) within the ±30° latitude band where warm-water coral reefs are found (Figure 1). Reefs in the Pacific and Indian Oceans tend to be dominantly wave forced (annual mean H_s > 1.5 m), whereas reefs in the Caribbean, Southeast Asia, and northern parts of Australia tend to experience only weak to moderate wave forcing (typical annual mean H_s < 1 m). These patterns likely drive substantial regional-scale differences in the wave-driven flows and residence times within reefs, depending, of course, on the morphologies of individual reefs within each region (Lowe & Falter 2015).

Despite the dominance of wave-driven reef systems globally, there are numerous reef systems worldwide that can be considered tide-dominated, defined here simply as locations where mean tidal range (*MTR*) exceeds annual mean H_s (Figure 1). Such systems have, for the most part, remained neglected in the literature; they include some extreme examples of macrotidal reef systems (*MTR* > 3 m) in regions off northern Australia, off east Africa, and off Central and South America (Figure 1). An iconic example of these tide-dominated reefs is the Kimberley region of northwestern Australia, where numerous reefs are subject to tidal ranges of ~10 m and water frequently drains off reef terraces during ebb phases of the tide (Purcell 2002). The dynamics of these tide-dominated reef systems are fundamentally different from those of traditional wave-driven coral reef flows, thus creating very different physical conditions within these reef habitats. As a consequence, the distinct environmental conditions within these tide-dominated reef habitats (such as in the Kimberley) would be expected to influence reef ecology, benthic productivity, and nutrient dynamics very differently from traditional wave-dominated tropical reefs.

The reefs of the Kimberley region of Western Australia are also one of the few remaining pristine coastal areas worldwide (Bryant et al. 1998, Halpern et al. 2008). The tidal regime of the west Kimberley causes reefs to undergo large fluctuations in environmental variables within a single tidal cycle. The purpose of this study was to estimate benthic fluxes of oxygen and nutrients and determine which environmental drivers (i.e., temperature, light) exert the strongest control on productivity. Understanding how variability in environmental conditions regulates the productivity of reef communities living in the western Kimberley provides a critical foundation for modelling and predicting both present productivity rates for reefs more broadly across the Kimberley, as well as how these rates may change into the future when environmental conditions change.

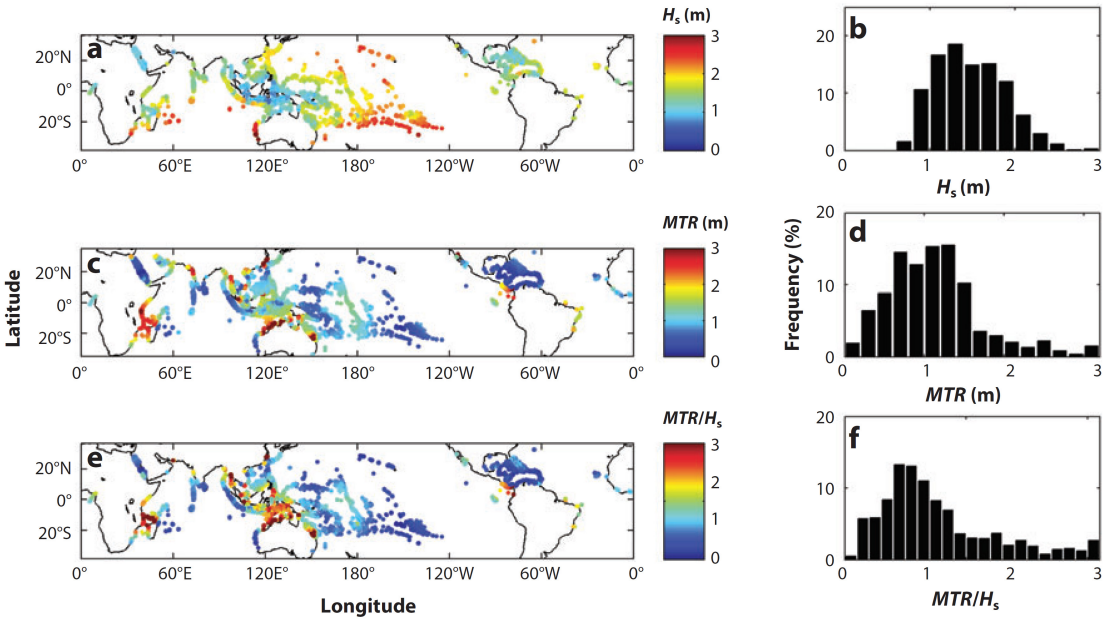

Figure 1. Global spatial distributions and frequency distributions of (*a*,*b*) annual mean significant wave height (H_s), (*c*,*d*) mean tidal range (*MTR*), and (*e*,*f*) relative tidal range (MTR/H_s) experienced by warm-water coral reef systems. Adapted from Lowe and Falter (2015).

2 Materials and Methods

2.1 Site selection

Reef systems of the Kimberley region of northwest Australia experience large and rapid variations in environmental conditions. Tides on the Kimberley coast are among the largest in the world, and ranges of up to 12 m have been measured in the central Kimberley (Kowalik 2004). Due to its complex ria coastline (Brocx & Semeniuk 2011), this region contains over 2600 islands, many with associated fringing reefs (Wells et al. 1995). The climate in northwest Australia is dry monsoonal, with rain primarily concentrated between November – March during the 'Wet' season, but with little rain during the rest of the year (the 'Dry' season). Human populations are sparse; thus, the Kimberley is among <4% of marine areas worldwide with little to no human impact (Halpern et al. 2008). These reef systems represent a unique opportunity to study pristine reef communities in a strongly tide-dominated setting. Though Australia's indigenous Traditional Owners have maintained ecological knowledge of these reefs for tens of thousands of years (Horstman & Wightman 2001), no studies have previously assessed the reef-scale productivity of these systems or the relationship between productivity and daily extremes in temperature, tide, and light.

The field study took place at Tallon Island (Figure 2), a high intertidal fringing reef located in the western Buccaneer Archipelago. This reef is characterised by its large platform (~1.5 km cross-shore), which sits slightly above mean sea level (0.25 m AHD) and experiences semi-diurnal tides of >8 m range during spring phases (Collins et al. 2015). The platform is nearly flat and its offshore boundary is sharply delineated by a steep crest (1-4 m high), over which water cascades during ebb tide (Lowe et al. 2015). This crest formation (coupled with bottom friction from benthic communities) is a hydraulic control for the draining reef and ensures that the platform remains submerged over a tidal cycle, despite the water level offshore falling up to several meters below the elevation of the reef (Lowe et al. 2015). Tidal duration is thus highly asymmetric on the reef platform, with ebb durations lasting ~10 hours regardless of phasing of the spring-neap cycle.

Although previous studies had recorded the dominant benthic species on Tallon Island reef (Wells et al. 1995), no map of benthic communities was available. The coverage of benthic community types on the reef platform

was determined by photographic transects during low tide. In the cross-shore direction, community type changed rapidly, so a 10-30 m spatial resolution was used, whereas a 100-200 m resolution was sufficient in the along-shore direction. Communities were characterised as being dominated either by seagrass or macroalgae (also containing coralline algae and small corals). This information was used to create a map of general habitat categories to guide site selection for experimental design and placement of equipment.

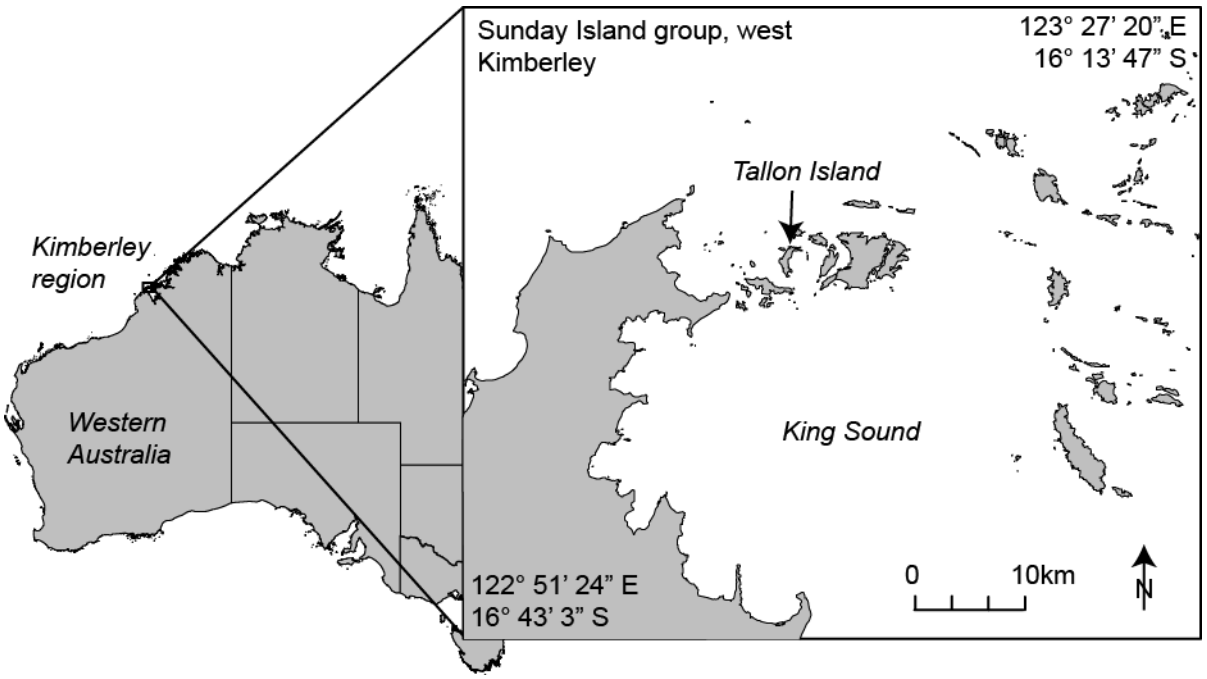

Figure 2. Location of Tallon Island reef study site in the Sunday Island group of the west Kimberley.

2.2 Field experiment #1 (2nd -22nd Oct 2013)

Our first field experiment was conducted on Tallon reef at the end of the dry season from 2-22 Oct 2013 involving 5 UWA staff and students, as well as Bardi Jawi Rangers and Traditional Owners. As part of this, the following instrument array was deployed throughout the reef (Figure 3):

- 3 dissolved oxygen (DO) sensors;
- 1 downwelling light sensor;
- 9 temperature sensors;
- 2 acoustic Doppler current profilers (ADP); and
- 4 pressure sensors.

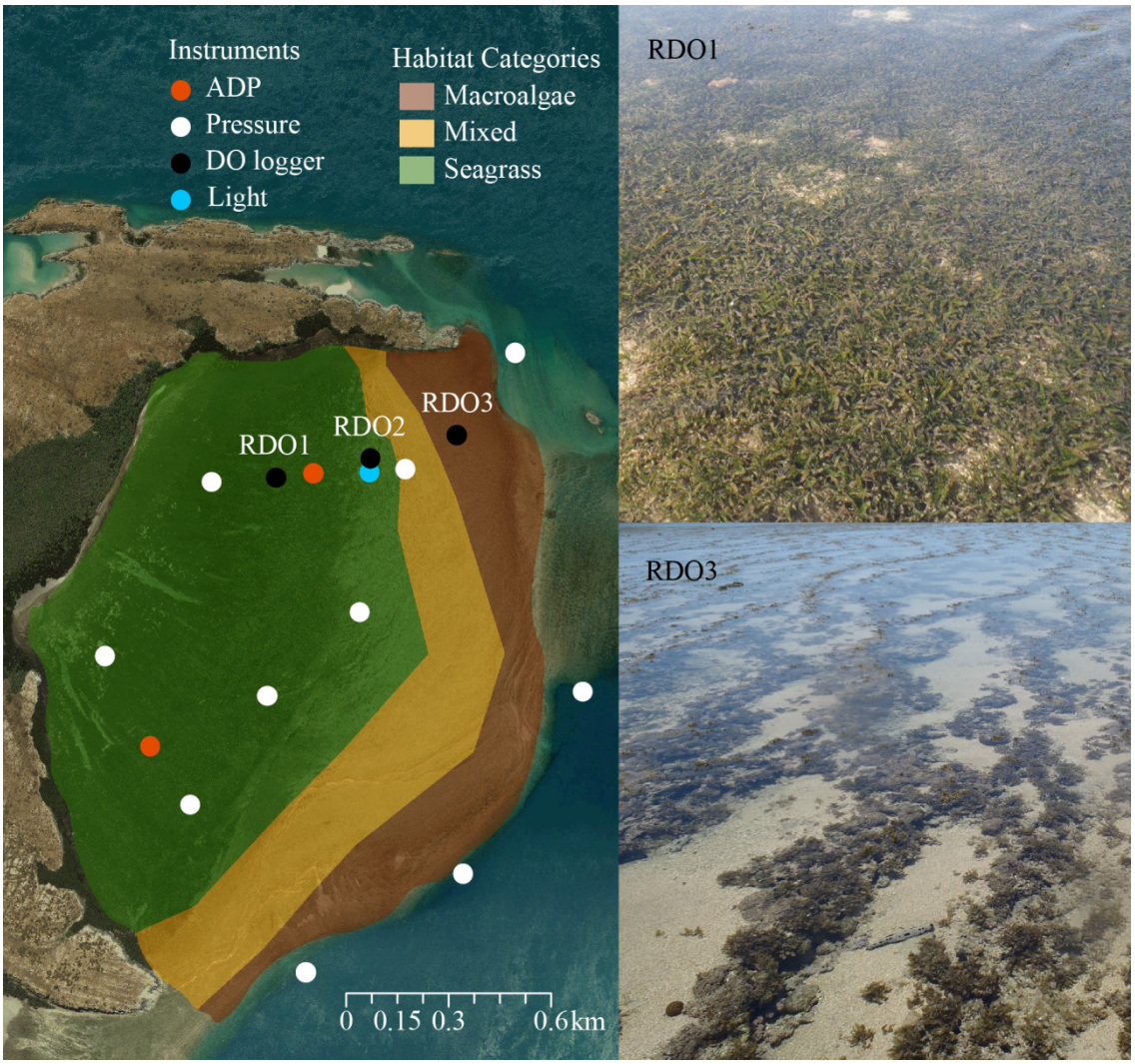

Figure 3. Instrument deployment locations (dots) on Tallon Island reef in zones of seagrass, benthic macroalgae, and mixed seagrass-algal (translucent colour). Water samples for nutrient and chlorophyll-*a* analysis were taken at the RDO stations (black dots). Images of benthic communities at dissolved oxygen loggers sites 1 (RDO1) and 3 (RDO3) during low tide are shown on the right.

Water levels and mean current velocities were sampled at 1 Hz by upward-looking 2 MHz Nortek Aquadopp current profilers (Nortek AS) weighted to the bed (Figure 4). A small vertical bin size (0.1 m resolution) allowed capture of current velocities when water levels were low atop the reef. A small neutrally-buoyant drifter (mandarin) was used to estimate water velocity during slow, nearly stagnant periods of low tide on the reef platform (Figure 5). The drifter was released repeatedly at each of the DO logger sites and allowed to travel for 30 min (n = 25).

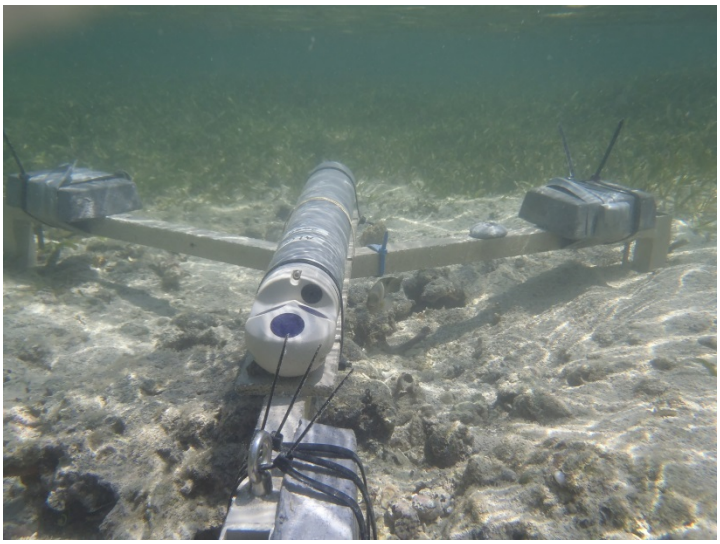

Figure 4. Acoustic Doppler current profiler deployed on Tallon reef, measuring three-dimensional velocity profiles above the reef.

Dissolved oxygen (DO) concentration was measured optically at 5 min intervals using Troll 9000 LTS packages (InSitu Inc.), which also logged temperature. Three DO sensors were deployed to capture conditions in the major reef communities: seagrass, algal ridge, and mixed assemblage (seagrass and algae). Sensors were located along the major axis of reef draining during ebb tide. DO sensors were calibrated before deployment using a two-point method of 100% (aerated with pump) and 0% (deoxygenated with sodium sulphite) saturation. In addition to pre-deployment calibration, DO measurements were corrected for drift by placing all loggers together for 30 min at periods during and after the deployment. Drift in DO measurements was minor ($\leq$ 0.32 mg L^{-1}) during the study. Due to sensor failure of one instrument, only estimates for the seagrass community were available during the first field experiment.

Light levels were directly measured at the Tallon Island study site. Downwelling photosynthetically active radiation (PAR) was recorded at the reef surface at 5 min intervals using a QCP-2300 cosine collector (Biospherical Instruments Inc.).

In addition to logger deployments, a suite of water quality parameters were measured at fixed stations on the reef (Figure 3). A fixed station in the adjacent channel was also sampled for comparison. Measurements of dissolved nutrients (ammonia, nitrate/nitrite, phosphate, total dissolved nitrogen and total dissolved phosphorus), particulate nutrients (particulate nitrogen and phosphorus), total suspended solids (TSS), and chlorophyll-*a* (chl-*a*) were undertaken regularly over 3 weeks.

Water samples for dissolved nutrients (25 mL) were filtered (0.45 μm Minisart syringe filter) on-site within 1 hour of being collected. Samples (2.3 L) for chla-*a* and TSS were shaken to homogenize and filtered using a vacuum pump onto pre-weighed and ashed (4 h at 550° C) filters (47 mm diameter 0.75 μm GF/F). Filters were rinsed with deionized water to remove salt and then placed in protective plastic containers for transport. Particulate nutrient samples were collected by passing 0.3-0.5L seawater through a filter (pre-ashed 25mm diameter 0.75 μm Whatman GF/F). Filters were retained, rinsed with ~5 mL deionized water to remove salt, and wrapped in foil for storage. All samples except TSS were immediately placed on ice after collection and then stored frozen at Cygnet Bay until transported back to Perth to be analysed within labs at UWA.

Figure 5. Lagrangian estimates of productivity are made by measuring oxygen concentration along drifter tracks over a seagrass bed. Mike Cuttler pictured.

During field experiment #1, benthic chamber measurements were also obtained during different parts of the light cycle to provide additional estimates of benthic productivity within beds of different seagrass species (i.e., *Thalassia* and *Enhalus*) and densities (i.e., dense and sparse). Clear chambers were used for estimates of net community production, while darkened chambers were used for estimates of net community respiration (Figure 6).

Figure 6. Oxygen concentration is measured in a clear chamber to estimate net community production in a *Thalassia* bed. Leonardo Ruiz-Montoya and Napo Cayabyab pictured.

2.3 Field experiment #2 (3rd – 10th February 2014)

A second field trip was conducted in early 2014 during the middle of the wet season involving 1 UWA student working closely with Bardi Jawi Rangers and a UWA volunteer. Road closures from heavy rain and difficulty shipping large amounts of research gear up the peninsula meant that this trip was at a much smaller scale than the others, and was mainly focused on measuring seasonal changes in water surrounding the reefs. Measurements of nutrients, chl-*a*, and total suspended solids were taken from the same fixed stations as Experiment 1 (Figure 3). In the last days scheduled for this trip, a large tropical low pressure system passed over Cape Leveque, requiring the research team to evacuate and ending this trip slightly early.

2.4 Field experiment #3 (22nd March – 12th April 2014)

A third field experiment was conducted on Tallon reef at the end of the wet season, involving 5 UWA staff and students. This experiment involved collaborative work with the Bardi Jawi Rangers, with Rangers participating on most days of the work. In addition, this experiment was conducted alongside an intensive hydrodynamic

study of the reef between UWA and CSIRO as part of project 2.2.1 on reef hydrodynamics, thereby providing very comprehensive hydrodynamic dataset that provided an opportunity to quantify in further detail how the reef hydrodynamics modify reef community productivity and nutrient fluxes in this project.

During these field experiments, the following instruments were deployed (Figure 3):

- 3 dissolved oxygen sensors;
- 2 optical fluorescence (chl-*a*) and turbidity loggers;
- 1 downwelling light sensor;
- 2 acoustic Doppler current profilers (plus 5 additional current measurements from 2.1.1);
- 2 pressure sensors (plus 8 additional pressure sensor measurements from 2.1.1);
- 64 temperature loggers; and
- ISCO automated water sampler (Figure 7).

Water sampling was conducted similar to field experiment #1, where samples were collected for the same parameters at fixed stations both across and off the reef, and with Lagrangian measurements from drifters (*n*=16). In addition, an automated water sampler was mounted on top of scaffolding (deployed for support of a weather station for project 2.2.1) to take water samples overnight for improved estimates of diel nutrient and chlorophyll-*a* fluxes (Figure 7). Wind speed and direction were measured 10 m above the reef during this study period.

Figure 7. Scaffolding atop Tallon Reef during high tide. Weather station and automated water sampler (ISCO) are also visible.

In addition, during this experiment we deployed a very high resolution array HOBO U22 Water Temp Pros (Onset) temperature loggers over the reef in a regular grid, in order to assess the drivers of spatial patterns of temperature variability and extremes, and how it relates to patterns of benthic productivity (Figure 8). Following Lentz et al. (2013), each temperature logger was calibrated in a controlled temperature water bath both before and after the deployment, such that the root-mean-squared errors were estimated to be <0.1^{o} C in all cases. The instruments were deployed on top of small lead weights (sampling ~0.1 m above the bed), and were also wrapped in white tape to minimize any solar heating.

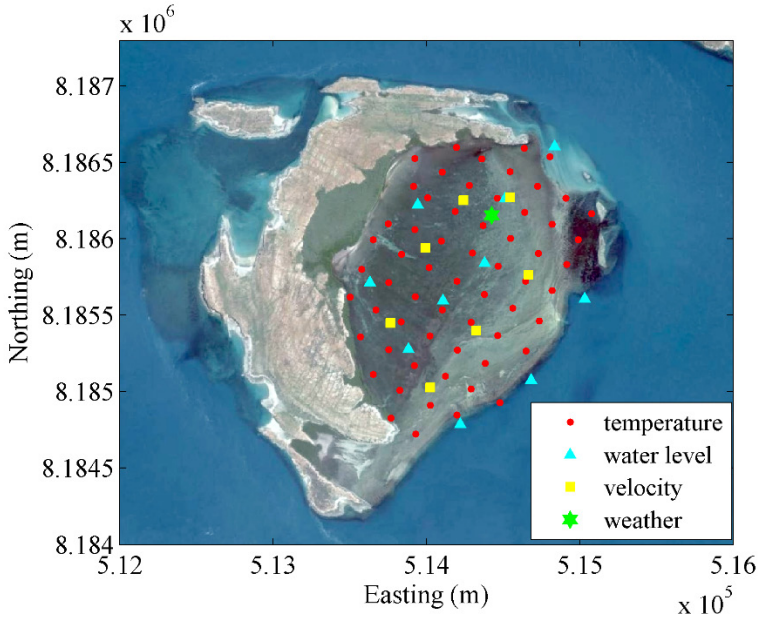

Figure 8. Location of the temperature data, weather station, and hydrodynamic measurements (combined with project 2.2.1)

2.5 Laboratory analyses

Samples of water column nutrients and chl-*a* from every field experiment arrived in Perth still fully frozen. At the laboratory, TSS filters were re-weighed to determine suspended solid concentration. Within one month of collection, chl-*a* filters were thawed, extracted in the dark with 100% acetone, sonicated, filtered, and analysed on a fluorometer (Turner Designs). Nutrient concentrations from water samples were determined through automated flow-injection analysis (LACHAT Quick Chem 8000). Particulate nitrogen filters were analysed using a Shimadzu CN analyser. Particulate phosphorus samples were digested in hot persulfate and concentrations determined colorimetrically on a spetctrophotometer (Shimadzu UV-Vis).

Differences in coastal water quality among seasons (Dry, Wet, late Wet) were tested using water samples taken from the channel adjacent to Tallon Island. Statistical significance ($\alpha = 0.05$) was determined with one-way analysis of variance (ANOVA), where data met assumptions of homoscedasticity and normality. Tukey-Kramer adjusted least-squared means were calculated and all possible pair-wise comparisons among seasons computed.

2.6 Community productivity estimates

The northern reef platform experienced flow in a consistent northeasterly direction during ebb tide (80° ± 30°, mean ± standard deviation) for ~10 hours each tidal cycle, with flow speeds becoming negligible as water depth became very low (<0.4 m) (Lowe et al. 2015). This prolonged period of unidirectional flow made the reef platform an ideal natural setting to capture community-scale (100s of meters) benthic oxygen fluxes. A one-dimensional control volume approach was taken with loggers placed along the major axis of ebb tide flow.

Depth-averaged flow speed along the major axis of the instrument transect (u_x) was available for all but ~5% of the field study, when water depth approached instrument blanking distance (h <0.4 m). For periods of low h, u_x was estimated from a significant linear relationship (p<0.001, R^2 = 0.79) between along-transect transport q_x and change in depth dh/dt (implied from conservation of mass, assuming horizontal dispersion was negligible) for 30-min averaged data from the Aquadopp and drifters (Figure 9). Transport was

$$q_x = u_x h \qquad (1)$$

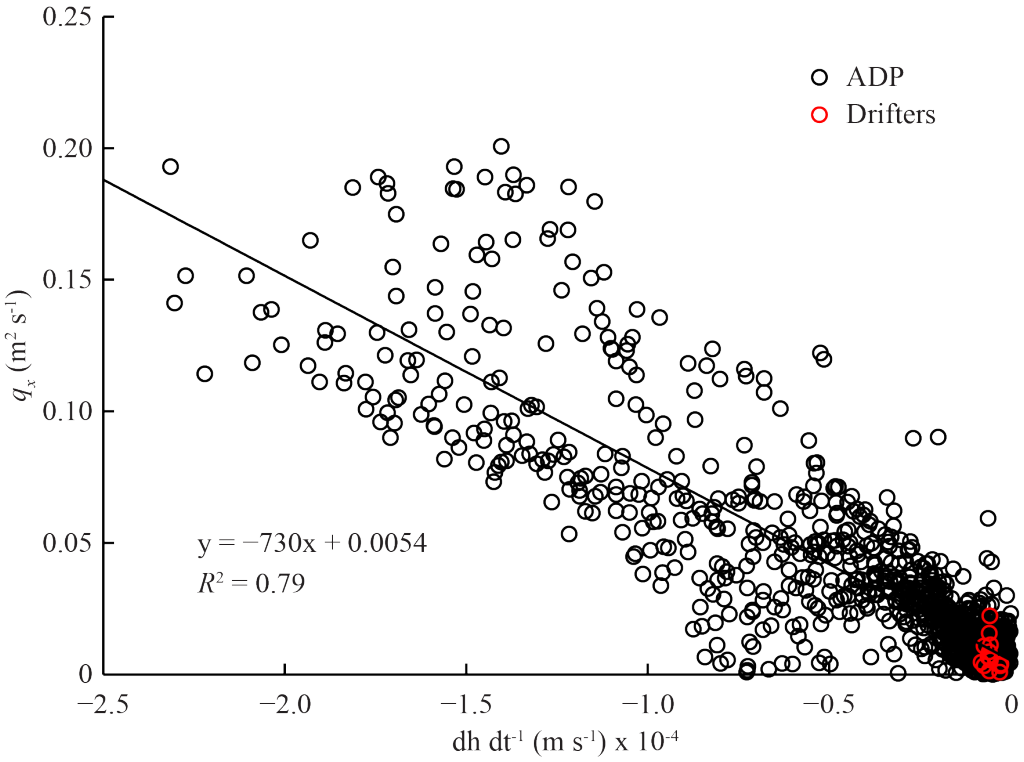

Figure 9. Linear relationship (significant at p<0.001) between transport (q_x) and rate of reef water level fall (during falling tide only) for measurements from the loggers (black) and the Lagrangian drifters (red).

Time-series of benthic oxygen flux (J_{O2}, in mmol O_2 m^{-2} hr^{-1}) were computed for the dominant communities (seagrass and macroalgae) from (Falter et al. 2011)

$$J_{O2} = \bar{h}\frac{d\bar{C}}{dt} + q_x\frac{dC}{dx} - k_{O2}(C_{sat} - \bar{C}). \quad (2)$$

The first term on the right side of the equation represents the local accumulation in oxygen concentration, where $\bar{C}$ is mean oxygen concentration along the transect (RDO1 and RDO2 for seagrass, RDO2 and RDO3 for macroalgae). The second term is the advective oxygen flux, where dC/dx is the gradient in oxygen concentration over the transect (dx is 270 m for both transects). The final term is the air-sea gas flux, where k_{O2} is the gas transfer velocity and C_{sat} is oxygen saturation estimated from water temperature and salinity (Weiss 1970). Previous work (Zappa et al. 2003, Borges et al. 2004) demonstrated that wind speed has a small effect on k_{O2} when speeds are low (<4 m s^{-1}), which occurred during the majority (~75%) of both field study periods. Estimates of gas transfer velocity that describe turbulent open channel flow were therefore more analogous to the reef platform than open-ocean studies. The reference gas transfer velocity k_{O2ref} was

$$k_{O2ref} = k_w + k_a, \quad (3)$$

the sum of gas transfer velocities due to water flow k_w and wind k_a (Chu & Jirka 2003). Flow-induced gas transfer was

$$k_w = 2.15(u^3{}_{*w}/h)^{0.25}, \quad (4)$$

where u_{*w} is bottom shear velocity defined as

$$u_{*w} = u_x\sqrt{C_D/2}, \quad (5)$$

and the drag coefficient C_D for the reef platform was taken as 0.02 (Lowe et al. 2015). Wind-induced gas transfer velocity k_a was

$$k_a = 0.00183u^2{}_{*a} \quad (6)$$

where u_{*a} is air surface shear velocity

$$u_{*a} = 0.01 u_{10} \sqrt{(8 + 0.65 \times u_{10})} \quad (7)$$

estimated from the wind speed at 10 metres (u_{10}) (Chu & Jirka 2003). Reference gas transfer coefficient k_{O2ref} was corrected to in situ conditions using estimated Schmidt numbers for oxygen under reference (Sc_{O2ref}) and in-situ (Sc_{O2}) conditions as

$$k_{O2} = k_{O2ref} (Sc_{O2ref} / Sc_{O2})^n \quad (8)$$

where n = 2/3 for a smooth air-water interface (Wanninkhof 1992). Schmidt numbers were estimated from a linear relationship with temperature (Ramsing & Gundersen 1994) as commonly-used estimates (Wanninkhof 1992) are only valid for temperatures <30° C. As wind speed measurements were not available for Oct 2013, the median wind speed from Apr 2014 was used to estimate k_{O2}.

Logged data were averaged at 30 min intervals for calculations of local and air-sea components of J_{O2}. The time-scale for averaging the advective flux term needed to reflect the transit time of a water parcel between oxygen loggers, which increased over the ebb tide period as u_x slowed and h decreased. For depths h > 0.90 m, the signal strength of J_{O2} was diluted by overlying water, so these periods were excluded from flux estimates. For 0.90 > h > 0.70 m, the advective flux term was estimated at 30 min intervals (Figure 10), which was roughly the transit time between loggers. As u_x slowed and 0.70 > h > 0.50 m, the advective flux term was estimated on a longer 80 min interval and linearly interpolated to the common 30 min interval used for all other terms. Towards the end of ebb tide, the depth became low (h < 0.5 m) and u_x became very slow (~1.5 cm s^{-1}); J_{O2} became dominated by the local accumulation term, though the advective term was included and estimated with 30 min averaged data. This method allowed for direct estimates of J_{O2} for ~50% of each field experiment. Due to the daily advancement of tides by 50 min, J_{O2} estimates covered a range of temperature and light conditions characteristic of this reef platform.

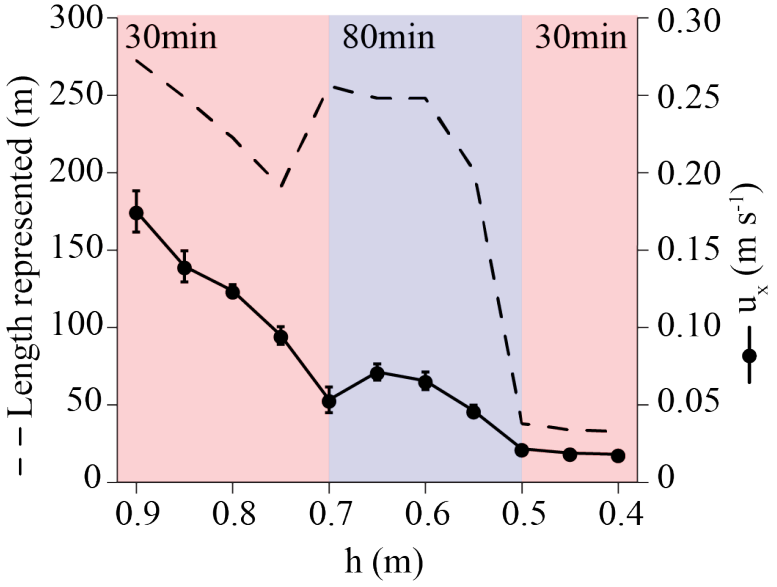

Figure 10. Length of reef incorporated in productivity measurements (dashed line) and mean ± standard error along-transect velocity (black dots) with changing water depth on Tallon reef. Coloured boxes indicate the time scale over which advective benthic flux calculations were made in order to best represent the benthic community of interest.

Daytime net production (NP in mmol O_2 m^{-2} hr^{-1}) was defined as J_{O2} occurring between sunrise and sunset (PAR > 5 μE m^{-2} s^{-1}), while nighttime community respiration rate (CR_{dark} in mmol O_2 m^{-2} hr^{-1}) was oxygen flux occurring between sunset and sunrise (PAR < 5 μE m^{-2} s^{-1}). Gross primary production rate (GPP in mmol O_2 m^{-2} hr^{-1}) was defined as

$$\mathrm{GPP} = \mathrm{NP} + \mathrm{CR_{light}} \quad (9)$$

where CR_{light} is the daytime community respiration rate (Staehr et al. 2012). Although it is common practice in metabolism studies to assume $\mathrm{CR_{light}} = \mathrm{CR_{dark}}$ (Cole et al. 2000), this assumption is unlikely to be valid given the extreme diel variations in temperature, flow, and DO characteristics of this site. It was therefore important to find an appropriate way to estimate CR_{light} given the above forcing factors.

The dependency of CR_{dark} on flow was examined with the maximum uptake rate coefficient of oxygen from mass transfer limitation (S_{MTL}) as (Falter et al. 2004),

$$S_{MTL} = \frac{\sqrt{cf/2}}{\mathrm{Re_k}^{0.2}\ \mathrm{Sc_{O2}}^{0.6}} u_x \quad (10)$$

where c_f is the friction coefficient, the Schmidt number of O_2 (Sc_{O2}) was the kinematic viscosity (v) divided by the diffusion constant of oxygen, and the Reynolds roughness number (Re_k) is defined as

$$\mathrm{Re_k} = u_{*w} k_s / v \quad (11)$$

where k_s is a bottom roughness length scale, assumed to be 0.5 m for the reef platform (Lowe et al. 2015). In reefs systems where water depth approaches the maximum reef organism height, c_f increases dramatically and can be estimated from empirical relationships to the ratio of h and maximum reef height (McDonald et al. 2006). First-order oxygen uptake rate coefficients (in m day^{-1}) for measured fluxes of CR_{dark} [where i = SG (seagrass) or AC (macroalgae)] were then estimated as (Thomas & Atkinson 1997)

$$k_i = CR_{dark} / \bar{C} \times 24 \quad (12)$$

and could be compared to S_{MTL}.

Respiration has an Arrhenius relationship with temperature often described by Q_{10}, the factor by which CR would increase if temperature were increased by 10°C (Berry & Raison 1981); in most aquatic systems (Valiela 1995) and for seagrass on Tallon reef platform (Pedersen et al. 2016), Q_{10} ~ 2. The degree to which temperature (T) changes likely affected CR was assessed by computing a temperature-adjusted version of CR_{dark} (CR_T) as (Burd & Dunton 2001)

$$\mathrm{CR_T} = \mathrm{CR_{dark}} + [\mathrm{CR_0} - \mathrm{CR_0} e^{\zeta(\mathrm{T}-\mathrm{T_0})}] \quad (13)$$

where CR_0 and T_0 were the mean CR_{dark} and temperature, respectively, when fresh ocean water was present on the reef at nightfall and $\zeta = \log_e(Q_{10})/10$.

The introduction of CR_T allowed analysis of patterns in CR_{dark} with the effect of temperature removed. A linear correlation between DO and CR_T was present in both reef communities (Atkinson et al. 1994) and was used to estimate CR_{dark} for instances of nighttime flood tides and CR_{light} using daytime DO levels (Figure 16). A saturating Monod-type relationship may also be appropriate (Zimmerman et al. 1989) and was plotted for completeness (Figure 16), though not used to estimate CR.

The relationship between GPP and irradiance was described by a hyperbolic tangent function (PI curves) (Jassby & Platt 1976). As discussed above, estimates of J_{O2} were not available during rising tide or periods of high water depth (h > 0.90 m), so GPP was estimated from PI curves using irradiance. Daily GPP (in mmol O_2 m^{-2} d^{-1}) was then calculated as the sum of all GPP (measured and estimated) in each day. Daily CR (in mmol O_2 m^{-2} d^{-1}) was similarly the sum of measured and estimated CR in each day. Net community production (NCP, in mmol O_2 m^{-2} d^{-1}) was daily GPP less daily CR.

Uncertainty in metabolism estimates due to random sampling error and statistical modelling error was quantified using the Monte Carlo method with 10000 sets of input variables. For variables directly measured in this study (T, h, DO, PAR, u_x, u_{10}), the standard deviation was drawn from the normally-distributed measurements used to create 30 min bin averages. For variables derived from statistical relationships (CR_{light}, GPP/CR_{dark} during high water depth), standard error of regression coefficients were used.

2.7 Reef heat budget analysis for Tallon reef

To assess the physical drivers of temperature variability over the reef, a reef heat budget model was derived from the integral form of the thermal energy equation that considers changes in the water temperature *T* within the reef, heat exchange by the advection of water on/off the reef, and the net surface air-sea heat fluxes Q_{net} (Kundu & Cohen 1990, McCabe et al. 2010):

$$\underbrace{\frac{d}{dt}\int_V T dV}_{\text{reef warming/cooling}} + \underbrace{\int_{A_{open}} T u dA}_{\text{heat advection}} = \underbrace{\frac{1}{\rho_0 c_p}\int_{A_{reef}} Q_{net} dA}_{\text{net surface heat fluxes}}, \tag{14}$$

which were evaluated over the reef control volume shown in Figure 11. Here ρ_0 is the seawater density, c_p is the specific heat capacity of seawater, A_{open} is the vertical perimeter area along the reef edge, A_{reef} is the plan area of the reef platform area and *V* is volume of water on the reef. Following McCabe et al. (2010), we simplify the model by assuming 1) the temperature is approximately uniform throughout the reef, i.e. $T(x,y,z) \approx T_r$ where T_r is a representative (spatially-averaged) reef temperature, and 2) that Q_{net} is likewise approximately spatially-uniform and that incoming water from of temperature T_{in} rapidly mixes with water on the reef.

Meteorological data was obtained using the weather station mounted on the scaffolding deployed on the reef (Figure 7). The weather station measured wind speed and direction, air temperature, relative humidity, barometric pressure and net solar radiation (via a radiometer) every minute. The radiometer was deployed on a horizontal pole ~1 m away from the scaffolding, and measured the net incoming and outgoing shortwave and longwave (infrared) radiation over the reef water surface (Q_{sw+lw}). Following an approach similar to Zhang et al. (2013), the meteorological and water temperature data were used to compute the individual terms that comprise net surface heat fluxes (Q_{net}), i.e.:

$$Q_{net} = Q_{sw+lw} + Q_{lt} + Q_{sb} \tag{15}$$

where Q_{lt} is the latent heat flux and Q_{sb} is the sensible heat flux. The latent and sensible heat flux terms were calculated using the COARE (Coupled Ocean Atmosphere Experiment) bulk algorithms (Fairall et al. 2003), as detailed in Zhang et al. (2013).

For a quasi-1D reef where water flows in/out of the reef approximately uniformly along the edge, the incoming/outgoing flow speed ($u_{in/out}$) can be estimated from the rate of change of the water level on the reef h_r according to mass conservation:

$$u_{in/out} = -\frac{A_{reef}}{W_r\left(h_r - h_{MSL,L}\right)}\frac{dh_r}{dt} \tag{16}$$

where W_r is the reef perimeter width and $h_{MSL,L}$ is depth of the back reef (or lagoon) relative to the reef crest (see Figure 1). With Eq. (16) and these uniform-property assumptions, the evaluation of the integrals in Eq. (14) lead to the following governing reef heat balance equation

$$\frac{d}{dt}\left(T_r h_r\right) - T_{in/out}\frac{dh_r}{dt} = \frac{Q_{net}}{\rho_0 c_p} \tag{17}$$

subject to the inflow/outflow temperature conditions

$$\begin{aligned} T_{in/out} &= T_0 \quad \text{if} \quad \frac{dh_r}{dt} \geq 0 \\ T_{in/out} &= T_r \quad \text{if} \quad \frac{dh_r}{dt} < 0 \end{aligned} \tag{18}$$

where T_0 is the surrounding (offshore) temperature and T_r is the reef water temperature.

Equation (18) was used to assess the reef temperature variability on Tallon reef and was also used to investigate the broader role of tides on reef heat balances. For Tallon reef, T_r and h_r were based on the spatially-averaged temperature and water depth, measured respectively by instruments on the reef, T_0 was from the temperature measured by instruments on the reef slope and Q_{net} was from the measured net heat fluxes. The numerical solution for T_r was obtained using Euler forward differencing.

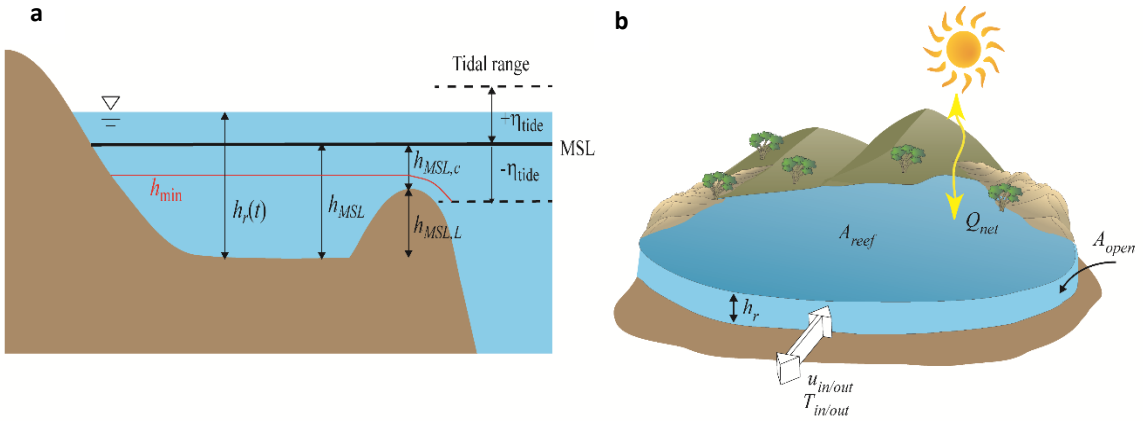

Figure 11. (a) Schematic diagram of a reef cross-section identifying the reef depth $h_r(t)$ that varies between a maximum amplitude (η_{tide}) above the depth h_{MSL} at mean sea level (MSL) and the minimum depth $h_{\min}$ of the lagoon/platform (refer to the text for details). The total depth h_r at the back of the reef (or lagoon) is comprised of the depth over the crest ($h_{MSL,C}$), if present, and the depth of the back of the reef relative to the crest ($h_{MSL,L}$). (b) Oblique view of a reef with surface area A_{reef} where water instantaneously exchanges over an area A_{open} between the reef and the ocean, with flow velocity $u_{in/out}$ and temperature $T_{in/out}$. Air-sea heat exchange on the reef occurs through Q_{net}.

2.8 General model of temperature variability in tide-dominated reefs

To more generally investigate how properties of the tide, solar cycle and reef morphology interact to regulate temperature variability within a wide range of reef systems, we recast the governing heat budget equations (Eqs. 17 and 18) into their dimensionless forms. To further simplify our analysis and identify a set of fundamental dimensionless parameters that control temperature variability, we consider idealized tidal and solar heating cycles that nonetheless retain the periodicity and magnitude exhibited by our in situ data. Variation in reef tidal depth (h_r) is thus assumed to occur at a tidal period of τ_{tide} with tidal amplitude η_{tide} (equivalent to one-half the range) and phase difference ϕ_0 relative to solar noon. The offshore mean sea level coincides with a reef depth h_{MSL} and we assume that there is a minimum water depth h_{min} where water is effectively trapped on the reef (Figure 11), i.e. this reef water depth variability is governed by

$$h_r(t) = h_{MSL} + \eta_{tide}\cos\left(\frac{2\pi t}{\tau_{tide}} + \phi_0\right) \tag{19}$$

with minimum depth $h_{\min}$ (such that $h_r \geq h_{\min}$ always), leading to tidal truncation for reefs with $h_{MSL} \leq h_{\min} + \eta_{tide}$. In this general model, we consider cases where the minimum depth $h_{\min}$ may be due to either water ponding within a shallower reef crest (in which case $h_{\min}$ is roughly equal to the mean lagoon

depth $h_{MSL,L}$ in Figure 11) or due to bottom friction restricting the flow of water off the reef (as in the case of Tallon reef). Likewise we assume a sinusoidal variation in the net surface heat flux term Q_{net} occurring with period τ_{solar}

$$\begin{aligned} Q_{net}(t) &= +Q_{net,max}\cos\left(\frac{2\pi t}{\tau_{solar}}\right) \quad t_{\text{sunrise}} \le t \le t_{\text{sunset}} \\ Q_{net}(t) &= -Q_{net,night} \qquad\qquad \text{at night} \end{aligned} \tag{20}$$

where $Q_{net,max}$ and $Q_{net,night}$ are the magnitudes of the maximum net daytime heating (mostly short and longwave radiation) and constant nighttime net cooling rates (mostly latent), respectively (see below). While this is an idealized representation of the diurnal heating cycle (see Results), it nonetheless captures the dominant diurnal behavior of the physics driving net heat fluxes within reefs (including Tallon), and has also been successfully used to model heat budgets and temperature variability within other reefs, such as in the GBR (McCabe et al. 2010).

With these definitions, we can further simplify our general heat budget model by constructing dimensionless variables (denoted with the *) for time (t^*), reef water depth (h_r^*) and temperature (T^*) to reduce the number of free parameters needed to constrain the prevailing physics:

$$t^* = \frac{t}{\tau_{solar}}, \quad h_r^* = \frac{h_r}{\eta_{tide}}, \quad Q_{net}^* = \frac{Q_{net}}{Q_{net,max}}, \quad T_r^* = \frac{T_r - T_0}{Q_{net,max}\tau_{solar}/\left(\rho_0 c_p \eta_{tide}\right)}, \tag{21}$$

where c_p and ρ_0 are the specific heat capacity and density of seawater, respectively, and by definition t^* is equivalent to one (solar) day. Substituting dimensionless variables into the governing Eqs. (17) and (18) then gives:

$$\frac{d\left(T_r^* h_r^*\right)}{dt^*} - T_{in/out}^* \frac{dh_r^*}{dt^*} = Q_{net}^* \tag{22}$$

with

$$\begin{aligned} T_{in/out}^* &= 0 \qquad \text{if} \qquad \frac{dh_r^*}{dt^*} \ge 0 \\ T_{in/out}^* &= T_r^* \qquad \text{if} \qquad \frac{dh_r^*}{dt^*} < 0 \end{aligned}, \tag{23}$$

where T_r^* and $T_{in/out}^*$ are the dimensionless forms of the reef water temperature and inflow/outflow temperature, respectively. For the idealized (sinusoidally varying) tidal forcing considered in Eq. (19), the reef water depth in dimensionless form becomes

$$h_r^*(t^*) = h_{MSL}^* + \cos\left(\frac{2\pi\tau_{solar}}{\tau_{tide}}t^* + \phi_0\right) \tag{24}$$

such that tidal truncation occurs when $h_{MSL}^* \le h_{\min}^* + 1$. From Eq. (20), the net surface heat flux term sinusoidally varies during the day (reaching a maximum $+Q_{net,max}$) and is constant at $-Q_{net,night}$ night; the constant night cooling rate was chosen to be equal to 25% of the daytime maximum warming rate $(Q_{net,max})$, which is typical of many tropical reef systems worldwide (McGowan et al. 2010, Davis et al. 2011, Zhang et al.

2013), including for Tallon reef in the present study (see Results). Therefore, the dimensionless net surface heat flux term becomes

$$\begin{aligned} Q^*_{net}\left(t^*\right) &= \cos\left(2\pi t^*\right) \qquad t^*_{sunrise} \le t^* \le t^*_{sunset} \\ Q^*_{net}\left(t^*\right) &= -0.25 \qquad \text{at night} \end{aligned} \tag{25}$$

Equations (22)-(25) can be solved using numerical integration to predict temperature variability on the reef as a function of the three dimensionless input parameters ($\tau_{tide} / \tau_{solar}$, h^*_{MSL} , $h^*_{\min}$) defined in Eq. (21).

3 Results

3.1 Reef communities

Tallon Island reef supported two distinct communities atop the reef platform: seagrass and macroalgae. The seagrass community was larger in area, stretching from the shoreline to ~400 m from the reef crest, and was dominated inshore by *Enhalus acoroides* (L.f.Royle) and offshore by *Thalassia hemprichii* (Ehrenb.) Aschers (Wells et al. 1995). The macroalgal community covered a band ~200 m wide at the reef crest and was dominated by brown macroalgae (*Sargassum* spp.) but also contained coralline algae, many macroalgal species, and small corals. A mixed assemblage of sparse *Thalassia* and *Sargassum* was found in the sandy ~200 m band separating seagrass and macroalgal communities (Figure 3).

3.2 Hydrodynamic context (current and water level variability)

A detailed study of tide-dominated reef hydrodynamics, including the hydrodynamics of Tallon reef, was the focus on Project 2.1.1. Therefore, only a brief summary of the main features of the current and water level variability on the reef are described here.

Field measurements captured a full spring-neap tidal cycle in both seasons, with tidal ranges of ~7 m during springs and ~2.5 m during neaps (Table 1). Water depth on the reef platform (*h*) ranged from 3.4 - 0.3 m during spring tides and from 0.3 – 1.3 m during neap tides (Figure 13a). Due to reef platform elevation 0.3 m above mean sea level, there were large asymmetries in duration of tide phases (Lowe et al. 2015). Ebb tide was elongated to ~10 h (Figure 12), with flow speed tapering from >0.4 m s^{-1} to 0.015 m s^{-1} over the ebb period (Figure 10). Wind speed (u_{10}) was generally low (Figure 13b) with a mean of 3.3 m s^{-1} (Table 1) and wind-driven waves did not occur due to the sheltering of Tallon Island by surrounding islands.

		Tidal range (m)		Wind speed u_{10} (m s^{-1})	Temperature (°C)		DO (μM)
Date	*n*	Spring	Neap	Mean ± SD	Mean ± SD	Range	Range
Oct 2013	14	6.7	2.6	nd*	28.5 (± 2.00)	25.5 - 36.6	491 - 20
Apr 2014	12	7.3	2.7	3.3 (± 1.56)	30.8 (± 1.47)	28.0 - 36.6	521 - 7

Table 1. Summary of environmental conditions on Tallon reef platform during both field experiments. *no data available

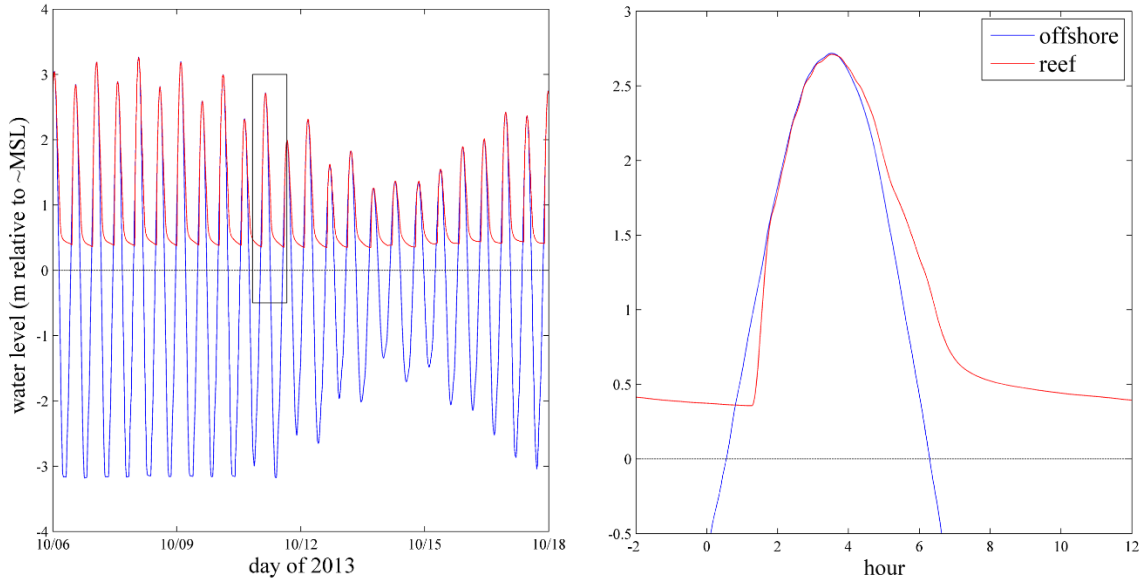

Figure 12. Water level (m relative to mean sea level) atop Tallon Reef platform (red line) and offshore (blue line). The full time-series from Experiment #1 is shown on the left, while the right shows a selected 12 hour period.

Environmental conditions on the reef platform were characterised by large diel changes, the magnitude of which was determined by the position of the solar cycle relative to the tidal cycle. Light levels were generally high, reaching 1800 μE m^{-2} s^{-1} when low water depth (h < 0.4 m) coincided with approximately mid-day. Water temperature on the reef platform was on average ~2° C warmer in the wet season than during the dry, though a wide range of temperatures were recorded during both seasons (Table 1). Temperature increases of >10° C within a single tidal cycle occurred when low tide coincided with high light levels (Table 1). Diel oxygen concentrations varied up to 440 μM (Figure 13c) and became supersaturated (> 100%) when low tide coicided with high light levels, reaching up to 280% saturation. Water column hypoxia (DO < 63 μM) developed on the reef platform each night for 1 - 7.5 h (Figure 13c), depending on the overlap of low tide and nighttime.

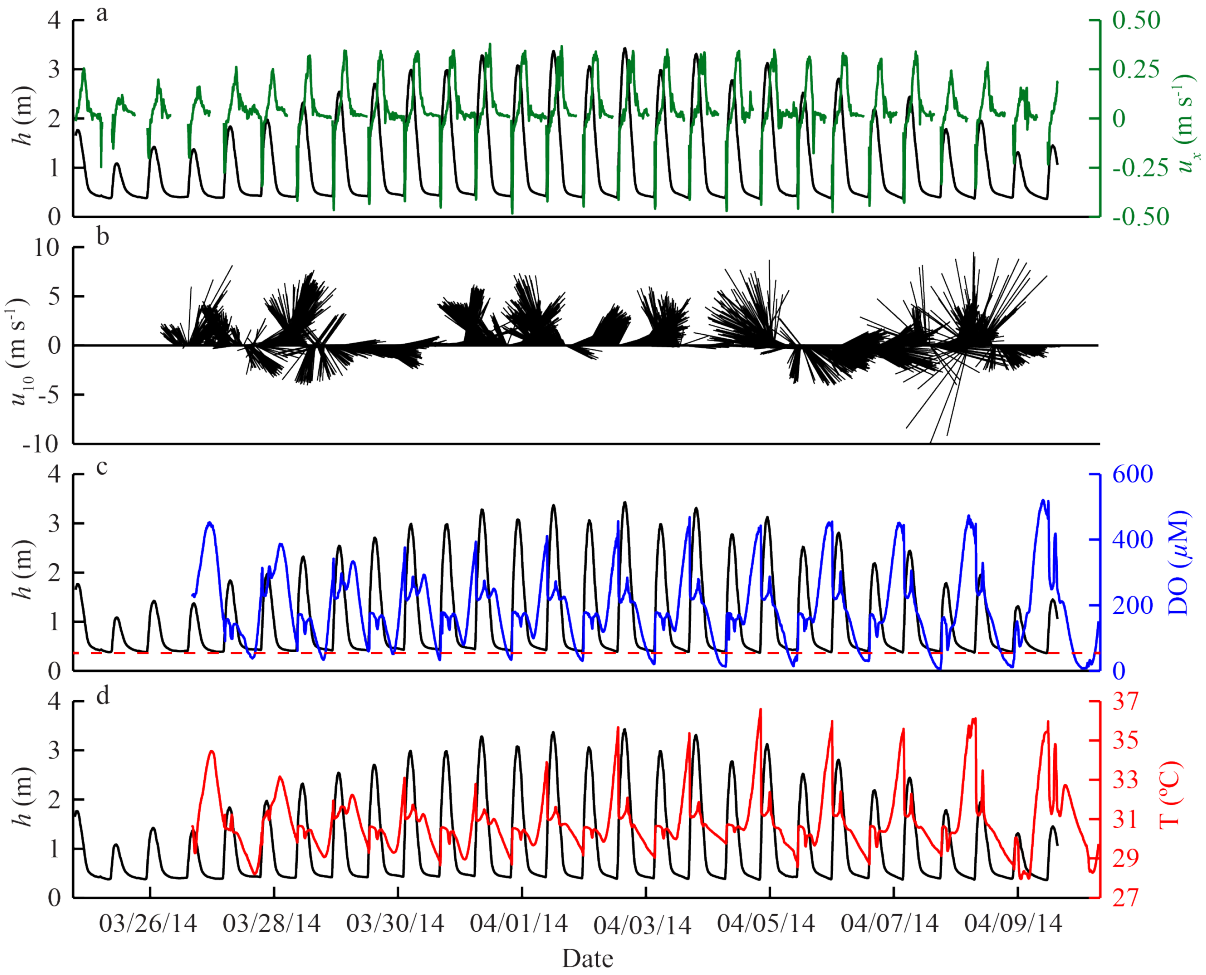

Figure 13. Time-series of conditions on Tallon Island reef during the wet season field experiment including: a) water depth on the reef platform (h, in black) and current speed in the along-transect direction (u_x, in blue); b) wind speed and direction at 10 m (u_{10}); c) dissolved oxygen concentration (blue) at RDO1 (seagrass site) with reef water depth (black); and d) water temperature (red) at RDO1 (seagrass site) with reef water depth (black). Red dashed line indicates hypoxia (DO < 63 μM).

3.3 Benthic community productivity

Environmental conditions and responses in benthic community metabolism were similar between seasons. In order to focus on metabolic response to environmental forcing, most results presented are from the wet season (Field Experiment #3) with implications of seasonality discussed towards the end. The relative importance of the three benthic oxygen flux components (local, advective, and air-sea exchange) to J_{O2} differed between benthic community zones (seagrass versus algae). In the seagrass community, overall J_{O2} estimates were dominated by the local accumulation term, with advective and air-sea components each contributing <10% (Figure 14A). Local and advective terms were both important to J_{O2} estimates in the macroalgal community (~55% and 35%, respectively), while air-sea exchange again contributed <10% (Figure 14B). Despite playing a minor role in overall J_{O2} estimates, air-sea exchange became important for short periods in the diel cycle, (e.g., when water column DO became supersaturated and flow was > 2 cm s^{-1}) (Figure 14B), and was therefore retained in the calculations.

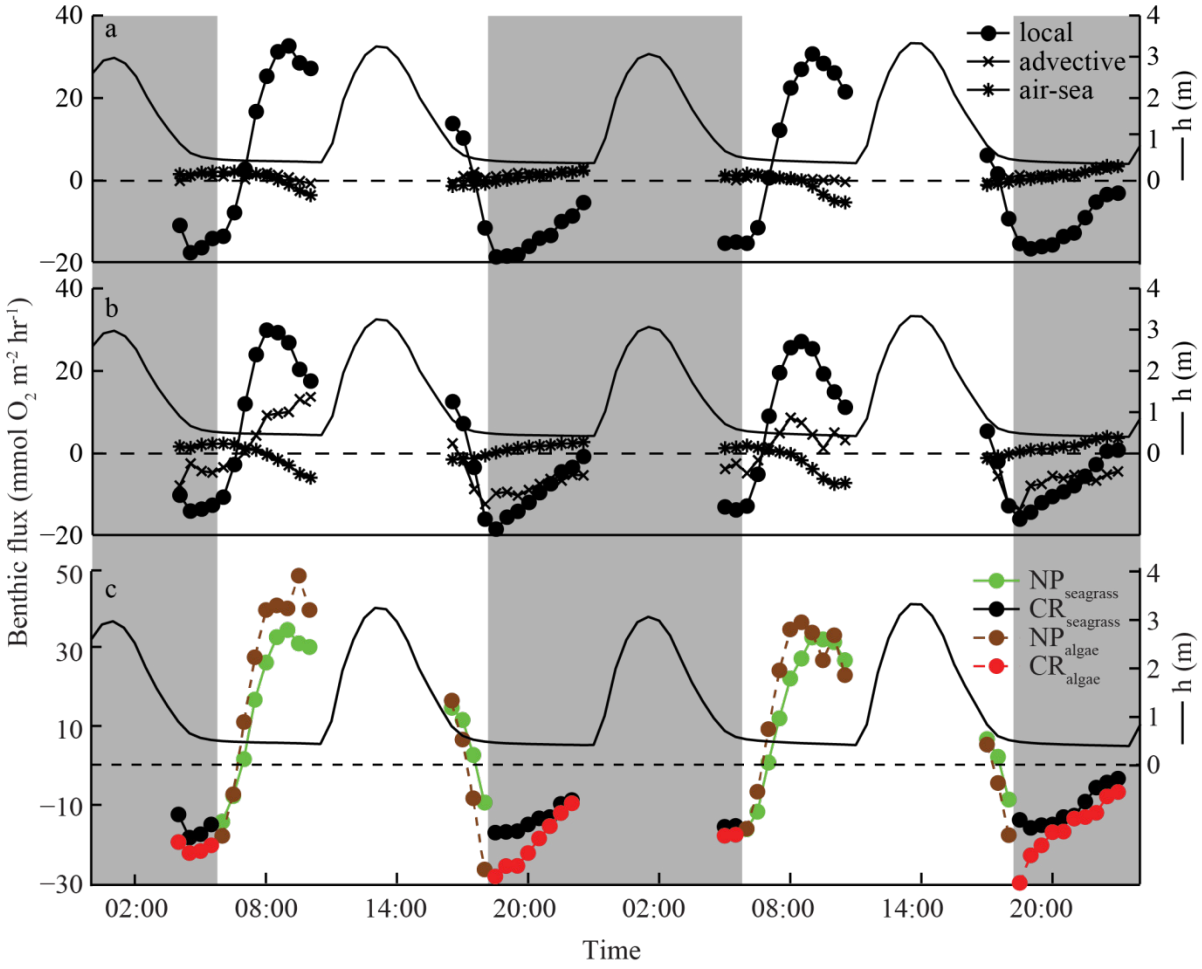

Figure 14. A two-day portion of the total time-series of local, advective, and air-sea components of J_{O2} for a) seagrass and b) macroalgal communities during the wet season field experiment with reef depth (black line). Hourly fluxes of c) NP and CR in both communities are shown with grey boxes denoting nighttime periods.

Hourly rates of reef community daytime net production and nighttime respiration showed distinct diel patterns (Figure 14C). The daily advancement of the tidal cycle by 50 min each day and length of both field studies resulted in metabolism estimates from a wide range of flow, temperature, DO, and light conditions characteristic of this reef platform. Comparison of first-order oxygen uptake rate coefficients derived from CR_{dark} (k_{SG} and k_{AC}) and those based on the limits of mass transfer (S_{MTL}) showed that CR_{dark} approached mass transfer limitation when flow speeds were low (Figure 15), but was not strongly related to flow speed in general.

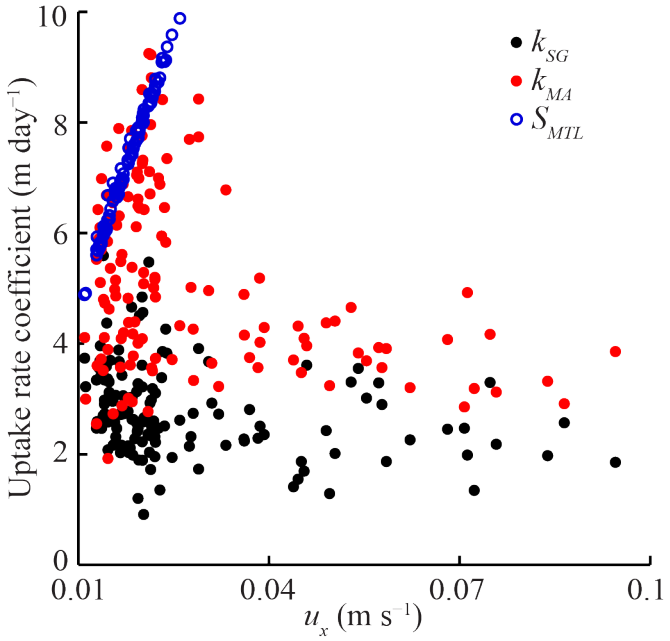

Figure 15. Relationship between flow speed (u_x) and first-order uptake rate coefficients of oxygen in seagrass and macroalgal communities (k_{SG} and k_{AC}), and coefficients estimated from mass transfer limits (S_{MTL}).

Rates of CR_{dark} tended to decline through the night, and approached zero when nighttime overlapped fully with ebb tide (Figure 14C). Water temperatures on the reef platform cooled by up to 4°C during these periods due to air-sea heat exchange. However, estimates of temperature-adjusted CR_{dark} (CR_T based on a Q_{10} = 2) demonstrated that only <8% of the pattern of decline observed in CR_{dark} could be attributed to falling temperatures. A strong linear trend was observed between CR_{dark} and DO in seagrass and macroalgal communities (p < 0.0001, R^2 = 0.73 and 0.61, respectively) over the range of DO (8 – 300 μM O_2, 10 – 150% saturation) measured (Figure 16). To assess whether depletion of labile photosynthates over the night could have contributed falling CR_{dark} (Figure 14C), this DO/CR relationship was also limited to only estimates from the first 2 hours after sunset, yet the linear trend remained similar.

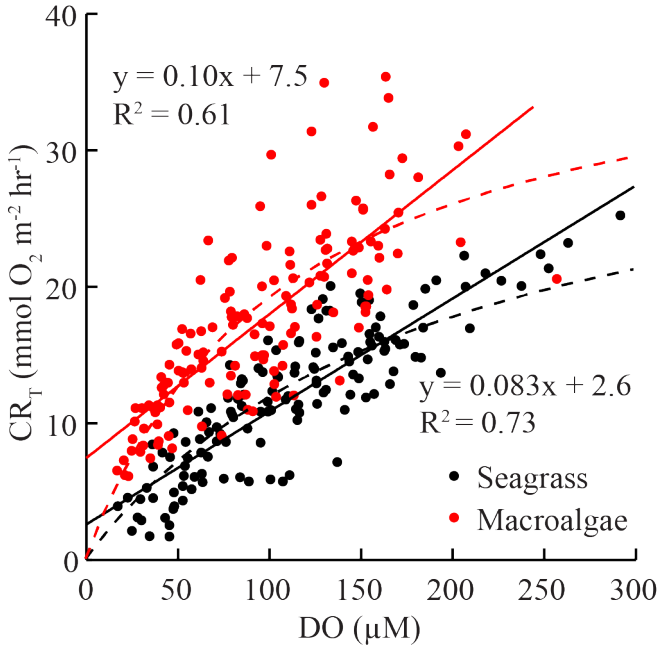

Figure 16. Relationships of temperature-adjusted CR_{dark} (CR_T) to water column DO in seagrass and macroalgal communities during the wet season field experiment. Equations and R^2 values shown are for linear relationships (solid lines), which were used to estimate CR_{light} and CR_{dark} for periods of high tide. Monod-type relationships (dashed lines) are also shown.

Due to the phase difference between light and tides, all light levels were represented equally (n = 20 for each 250 μE m^{-2} s^{-1} increment of PAR) during the experiments. Photosynthesis-irradiance curves made using

estimates of net daytime production (NP) from field measurements (as opposed to statistical relationships) revealed responses related to DO (Figure 17). Hourly net production rates were greater overall in the macroalgal community than the seagrass community (Figure 17). Both communities showed declining rates of NP when DO was high (>350 μM), which typically occurred in the afternoon and indicated some hysteresis in NP.

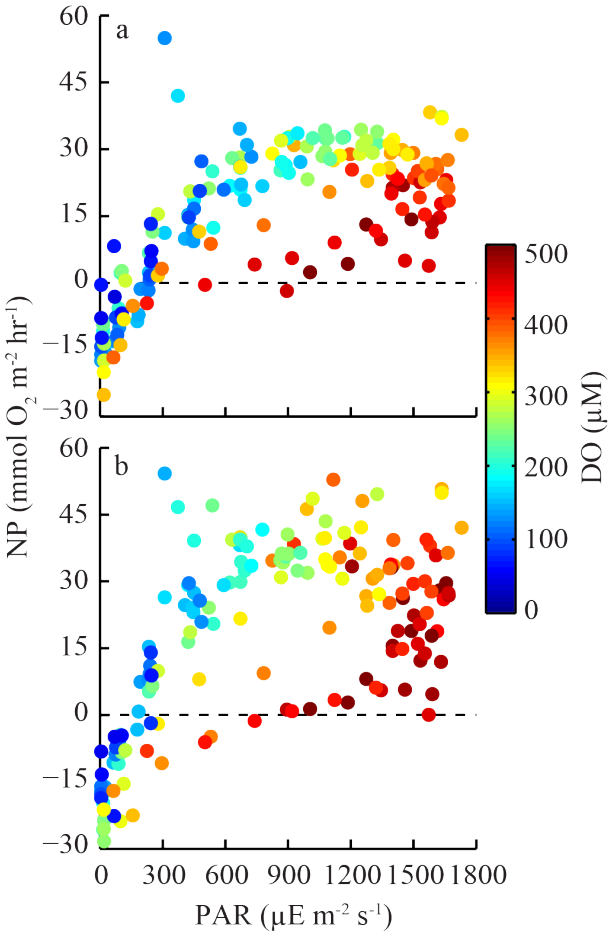

Figure 17. Photosynthesis-irradiance (PI) curves for net production in a) seagrass and b) macroalgal communities during the wet season field experiment. Water column DO for each measurement is shown in the colorbar.

Daytime community respiration rates (CR_{light}) were estimated based on linear relationships with DO (Figure 16) and used to calculate rates of hourly gross primary production (Figure 18). Like NP estimates, the macroalgal community showed greater rates of GPP than seagrass at all light levels. Photosynthesis-irradiance relationships using GPP exhibited a classic hyperbolic tangent form, with no hysteresis evident (Figure 18). This indicated that the pattern of hysteresis observed in NP at high light levels (Figure 17) was driven by increases in daytime CR relative to photosynthesis.

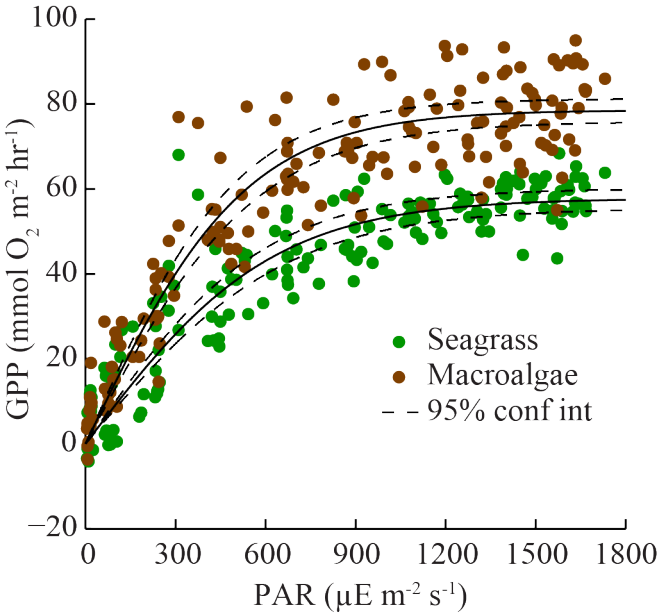

Figure 18. Photosynthesis-irradiance curves for hourly rates of GPP in seagrass and macroalgal communities during the wet season field experiment. Best hyperbolic tangent fit (solid lines) are shown with 95% confidence intervals (dashed lines).

Mean daily rates of metabolism (the combination of field measurements and estimates from statistical models) showed similar net community production between seagrass and macroalgae (Table 2). The macroalgal community had higher overall rates of both GPP and CR than seagrass, yet both communities had balanced P:R ratios over the whole experiment (Table 2).

Community	*n*	NCP	CR	GPP	P:R
Seagrass	12	50 (± 7)	440 (± 4)	490 (± 5)	1.1
Macroalgae	12	30 (± 8)	670 (± 4)	700 (± 5)	1.0

Table 2. Summary of daily net community production (NCP), community respiration (CR), and gross primary production (GPP) during the wet season. Daily fluxes (mean of *n* days) in units of mmol O_2 m^{-2} d^{-1} (± standard error). Ratio between daily GPP and CR (P:R) also shown.

NCP also varied on a daily basis due to changes in environmental forcing (Figure 13) driven by the mismatch between the length of tide and light cycles (50 min daily). This is best visualized by plotting daily NCP as a function of the phase difference between light and tide on that day (Figure 19). A phase difference of 0° represents a day when high tide was aligned with solar noon/midnight, and thus ebb tide occurred from ~12:00 – 22:00 and 0:00 – 10:00. A phase difference of 180° represents a day when high tide was aligned with ~18:00/6:00, and thus ebb tide occurred from ~18:00 – 04:00 and ~6:00 – 16:00. Maximum daily NCP was observed near ~0° and decreased as tide-light phase difference advanced, reaching a minimum near ~180° (Figure 19). A phase difference of 180° means that the water depth was low when the highest light levels occurred, resulting in large increases in DO and temperature on the reef platform. This strong cosinusoidal pattern in NCP was seen in both communities over wet and dry seasons (Figure 19).

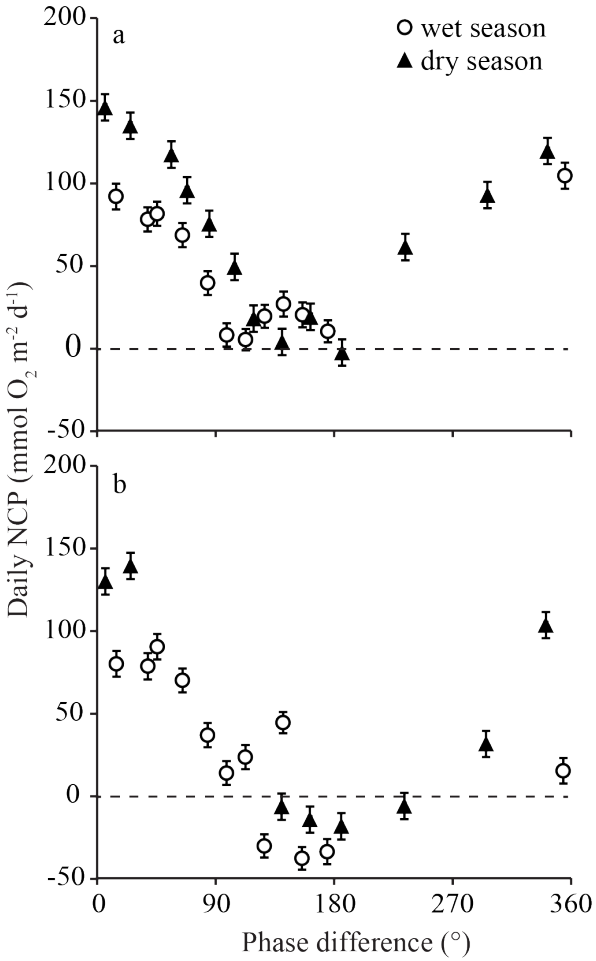

Figure 19. Mean (± SD) daily rates of net community production (NCP) in a) seagrass and b) macroalgal communities during both seasons. Rates are shown as a function of the phase difference between light and tide cycles, with 0° indicating alignment of high tide and solar noon.

3.4 Nutrient and chlorophyll-*a* dynamics

Changes in dissolved nutrient concentration due to uptake and release by benthic communities were most readily measureable during slow flow speeds (u_x) occurring in low tide periods. In the macroalgal-dominated zone, strong signals of dissolved inorganic nitrogen release as nitrate/nitrite (NO_x), and ammonia (NH_3) were measured, whereas seagrass communities showed slight nitrogen uptake (decrease in concentration) (Figure 20). In both community zones, phosphate (PO_4^{3-}) concentrations remained stable during low tide periods and were similar on and off the reef platform (Figure 20C). Offshore samples were taken from all phases of the tidal cycle, and there was no difference in nutrient concentration with phase of tide.

By utilizing the one-dimensional control volume approach described previously to measure community productivitiy, we were able to estimate nutrient uptake or release rates during ebb tide periods. Release rates of NO_x increased through the ebb period, reaching a maximum in the late afternoon (Figure 21). Ammonia uptake and release rates were lower overall than NO_x by an order of magnitude. There was net community uptake of NH_4^+ early in the ebb tide period, which switched to net release around midday. Phosphate uptake / release rates were negligible.

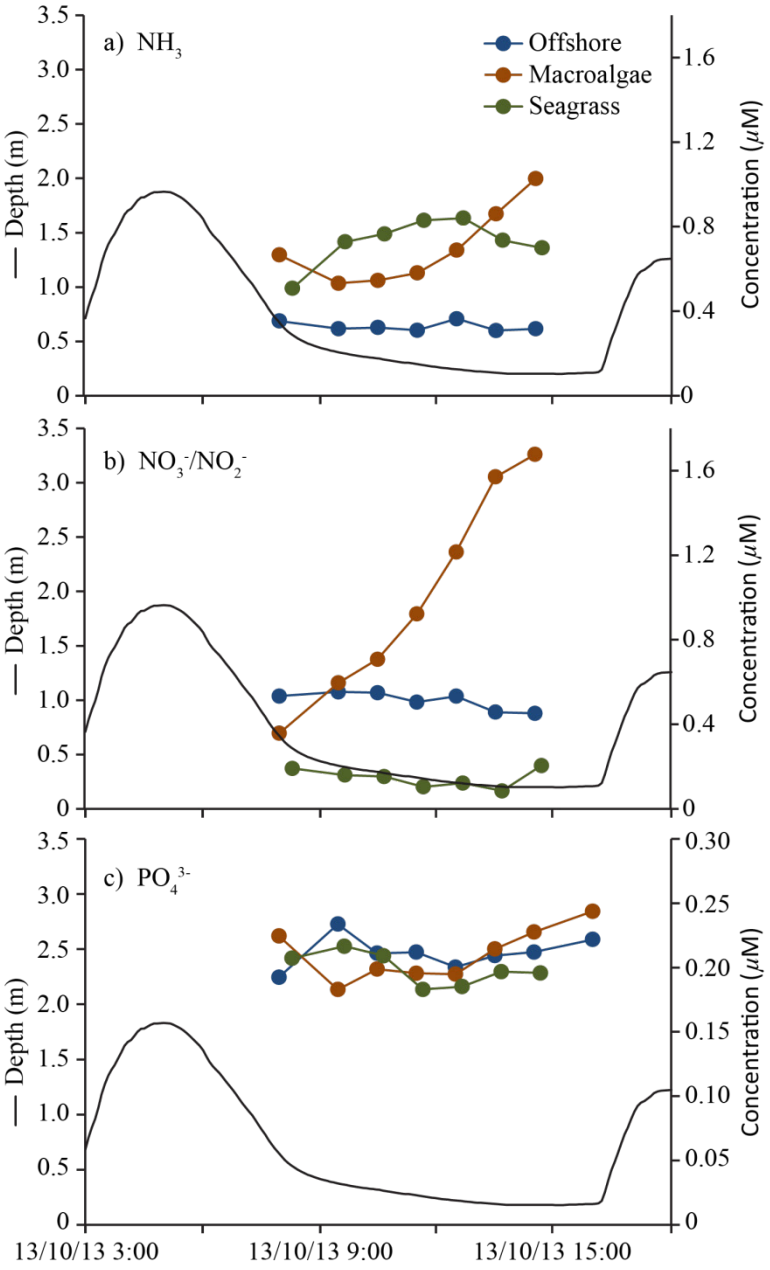

Figure 20. Representative time-series of water column dissolved a) ammonia, b) nitrate/nitrite, and c) phosphate concentration over an ebb tide period during the dry season. Samples taken from offshore reference (blue), macroalgae-dominated (orange), and seagrass-dominated (green) communities. The depth of water on Tallon reef is shown (black line).

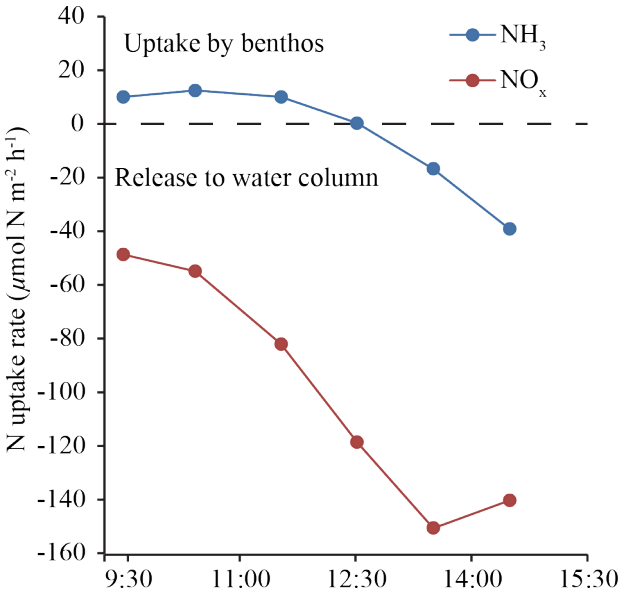

Figure 21. Representative time-series of nitrate/nitrite (red) and ammonia (blue) uptake rates during a single ebb tide period during the October 2013 field experiment. Positive values indicate nutrient uptake, while negative values indicate nutrient release to the water column.

Using the automated water sampler during Field Experiment #3 in the late-wet season, we were able to measure water quality changes over full diel and tidal cycles. These measurements were used to verify logged data from optical chl-*a* sensors deployed on the reef platform. Suspended chlorophyll-*a* (mainly from phytoplankton, but also including small plant-derived detritus) is a primary food source of reef filter-feeding organisms. Chlorophyll-*a* concentration showed substantial variability over each tidal cycle, with peaks in concentration occurring near peak flood and ebb velocities, presumably due to resuspension and mixing on the reef platform (Figure 22). Flood tides also flushed fresh suspended labile material onto the reef flat, which was then grazed down almost to zero during ebb tide (Figure 22).

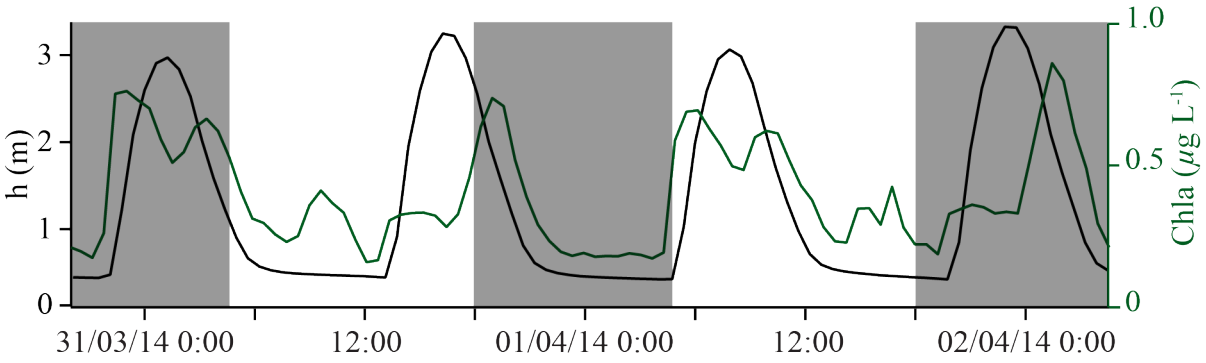

Figure 22. Representative time-series of chlorophyll-*a* concentration (green) and water depth (black) over two full days during the wet season field experiment. Nighttime periods are marked with grey boxes.

Seasonal differences in water quality in the vicinity of the reef platform were evident despite strong mixing in channels surrounding Tallon Island. Concentration of dissolved inorganic nitrogen species (nitrate/nitrite and ammonia) increased significantly through the wet season, while phosphate concentrations did not change significantly (Figure 23A). Chlorophyll-*a* and phaeophytin (suspended dead photosynthetic material, mainly comprised of dead phytoplankton) levels also increased significantly through the wet season (Figure 23B). Ratios of chl-*a* to phaeophytin indicated that the majority of suspended photosynthetic material was detrital in

nature.

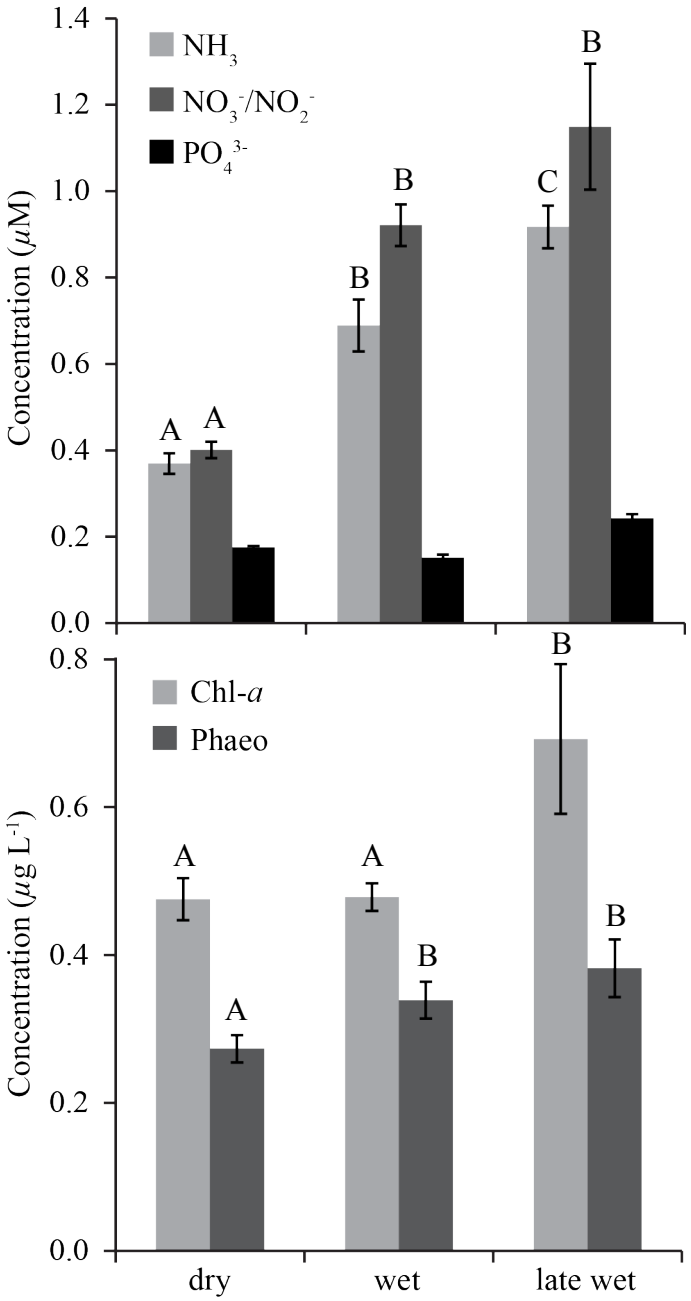

Figure 23. Offshore concentration of water column dissolved nutrients (ammonia, nitrate/nitrite, and phosphate), chlorophyll-*a*, and phaeophytin during all field experiments. Values are means with standard error. Uppercase letters indicate statistical significance at $p < 0.05$ among seasons.

3.5 Role of interacting tidal and solar heating cycles on temperature variability

3.5.1 Tallon reef temperature and heat flux observations

During Field Experiment #3 when a detailed reef heat budget for Tallon was quantified, the offshore tidal range reached a maximum of ~7.5 m near the middle of the study during spring (~1 Apr) and a minimum of ~4 m during neap towards the beginning and end (Figure 24a). Water levels over the reef platform were highly asymmetric, with water draining very slowly off the reef during ebb tide, as a result of the large 'truncation' of tidal variability over the reef (i.e. the duration of the ebb was ~10 hours while the flood was only ~2 hours) (Figure 24a). Due to the 12.4 hour period of the dominant M2 tide, the time of the offshore low tide minima

gradually shifted forward over the study period. Initially, the first low tide of the day occurred prior to sunrise and gradually shifted to just before noon by the end of the experiment (Figure 24d).

Diurnal variations in the net surface heat fluxes Q_{net} did not vary substantially over the course of the experiment, typically ranging from -200 W m^{-2} at night to +600 W m^{-2} during the day (Figure 24b). This consistency was due to the cloud-free skies that persisted over most of the experiment; conditions that are typical during the 'dry season' in the Kimberley (April through October) due to its tropical monsoon climate. Variations in Q_{net} were dominated by net heating from the combined short and long wave radiation (Q_{sw+lw}) during the day and net cooling from latent heat fluxes (Q_{lt}) during the night (Eq. (15)).

Daily temperature fluctuations in reef water temperature T_r (spatially-averaged over the reef platform) ranged from as small as ~2° C during the initial period of the study, to as large as ~8° C during the latter period and exhibited fairly complex but periodic behavior (Figure 24c). Nonetheless, our simple reef heat budget model (Eqs. (17)-(18)) was able to accurately reproduce both the shape and magnitude of the complex diurnal temperature reversals over the course of the study. The maximum diurnal temperature fluctuations were greatest towards the end of the study when low tide occurred slightly before solar noon despite the tidal range being lower at this time (Figure 24d). Therefore, the maximum observed temperature fluctuations were not in phase with the maximum daily tidal amplitude (Figure 24a,c); i.e., diurnal temperature fluctuations were not maximal during the largest spring tides. This is because once the offshore sea level drops below the reef crest, the depth and duration of the remaining ebb tide period on the reef is determined solely by the morphology of the reef regardless of how low offshore sea levels reach (i.e., -2 m during neap vs. -4 m during spring). More generally, we find that the phase difference between the semi-diurnal (M2) tide and solar cycles generally has the most substantial influence on the reef heat balance, such that the magnitude of daily temperature variation ($\Delta T_r = T_{\max} - T_{\min}$, where T_{max} and T_{min} are the daily temperature maxima and minima) is mostly independent of the spring-neap phasing at Tallon Island.

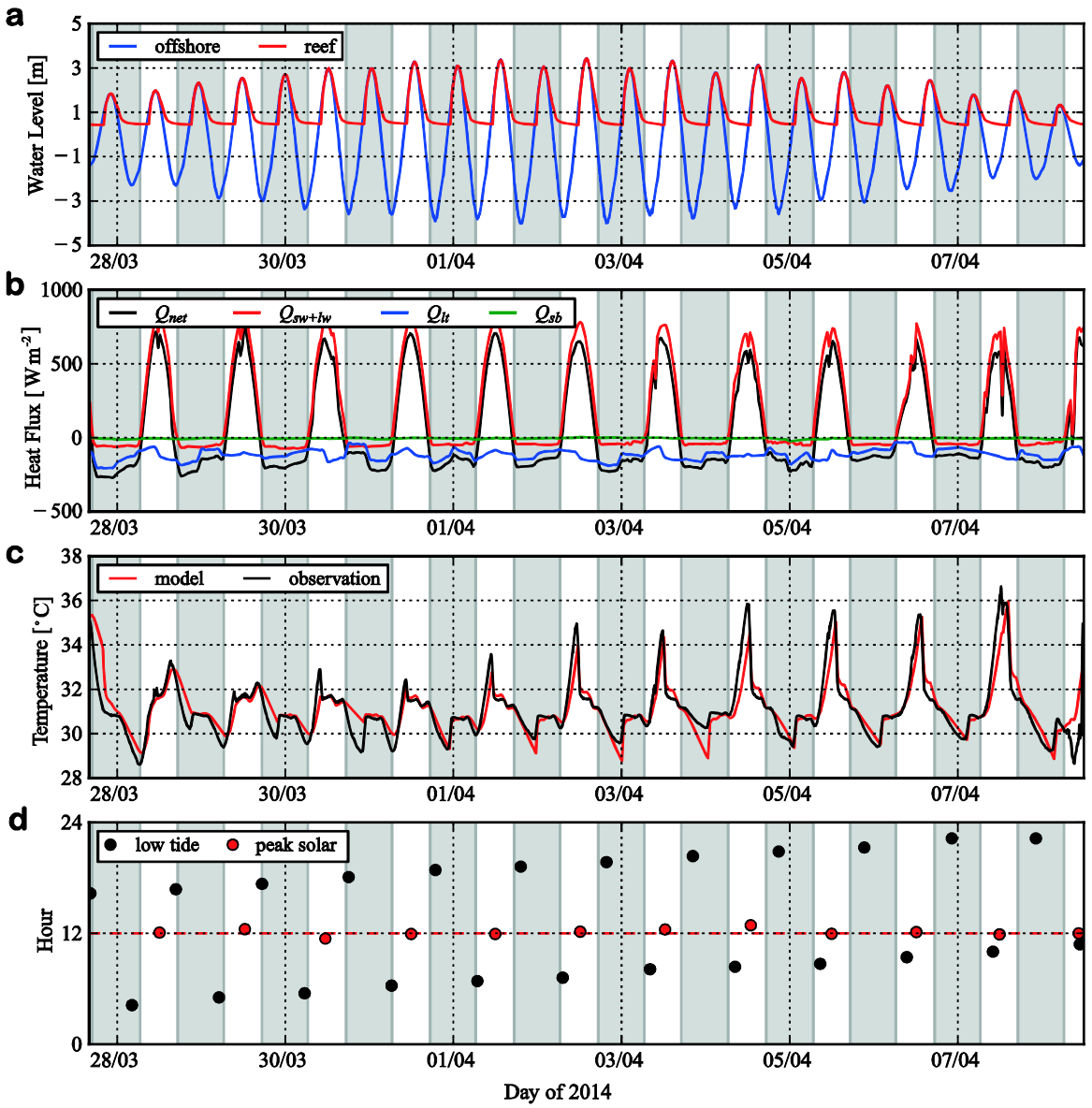

Figure 24. Observations and model predictions of the reef heat budget for Tallon Island during the field study period. (a) Time series of the water level variability (relative to mean sea level) measured at a site on the reef platform (red) and at a site offshore on the forereef slope (blue). (b) Terms that comprise the total net air-sea heat fluxes Q_{net}, including the combined net short- and long-wave radiation (Q_{sq+lw}), latent (Q_{lt}) and sensible (Q_{sb}) heat flux contributions. (c) The observed spatially-averaged reef temperature T_r compared with the model predictions. (d) The hour of day when minimum low tide measured offshore occurred and when peak solar irradiance occurred each day. The horizontal red dashed line corresponds to the mean hour of peak solar irradiance during the study at approximately noon.

3.5.2 *Model predictions of Tallon reef temperature variability*

To further demonstrate the general responses of the model and assess how tides and solar heating cycles drive temperature variability on these macrotidal reefs, we first consider the application to a simplified Tallon reef where $h_{\min}$ = 0.5 m and h_{MSL} = 0 m, the tide consists solely of an M2 mode (the dominant mode at Tallon) such that $\tau_{tide} = 12.42$ hr, and a tidal amplitude η_{tide} = 3 m that is halfway between the spring maxima (4 m) and neap minima (2 m); the results of which yield $\tau_{solar} / \tau_{tide} = 0.52$, $h^*_{MSL} = 0$ and $h^*_{\min} = 0.17$ (Table 3). To

assess the variability in T_r^* over multiple tidal cycles (days), we initialize each simulation with $\phi_0 = 0^o$ and advance forward in time, such that there is an additional 0.84 hr (~50 min) lag in the solar cycle relative to the tidal cycle each day. The results reveal the presence of a low frequency modulation of the diurnal fluctuations in T_r^* with a beat period of $\tau_{low} = \tau_{solar}\tau_{tide} / \left(2\tau_{tide} - \tau_{solar}\right) \approx$ 14.8 days, which are generated by the daily phase drift between the M2 tide and the diurnal solar cycle (Figure 25a). Importantly, while this low frequency modulation of temperature occurs at the same frequency of spring-neap tidal cycles, which are governed by analogous interactions between solar and lunar tidal constituents (Kvale 2006), the temperature variability here is generated solely by interactions between solar heat fluxes and the dominant lunar tides (since the daily tidal amplitude here is constant).

Label	Site	η_{tide}	$h^*_{\min}$	$h^*_{MSL} = h_{MSL} / \eta_{tide}$		
				present	**MSL +0.7 m**	**MSL +1.5 m**
Ⓐ	Tallon Island, Kimberley, northwestern Australia	3.0 m	0.17	0.00	0.23	0.50
Ⓑ	Warraber Island, Torres Straight	1.2 m	0.33	0.33	0.92	1.58
Ⓒ	Cocos (Keeling) Islands, eastern Indian Ocean	0.6 m	0.42	0.42	1.58	2.92
Ⓓ	Lady Elliot, Great Barrier Reef	0.8 m	0.50	0.50	1.38	2.38
-	Ofu, American Samoa	0.5 m	2.00	2.00	3.40	5.00
-	Rarotonga, Cook Islands	0.4 m	2.50	2.50	4.25	6.25

Table 3. Tidal amplitudes and reef morphology parameters for Tallon reef and other example tidally-forced reefs globally. Values of dimensionless reef depth relative to mean sea level (h^*_{MSL}) are included for present conditions (0 m MSL) and two sea level rise scenarios (+0.7 m MSL, +1.5 m MSL).

We can use the Tallon reef example ($h^*_{MSL} = 0$ and $h^*_{\min} = 0.17$) to further investigate how the magnitude of the maximum diurnal temperature fluctuations ΔT_r^* (defined as the difference in the daily maximum and minimum of T_r^*) plotted for different instantaneous phase differences $\Delta\phi_i$ between the solar and tidal cycles

(Figure 25b). Here $\Delta\phi_i$ is defined as the instantaneous phase mismatch between the maximum tide and solar noon on a given day. The maximum dimensionless temperature fluctuation ($\Delta T_r^* \approx 1.8$) occurs when $\Delta\phi_i$ is slightly less than 180° (roughly equivalent to when low tide occurs just before solar noon), which defines a general condition of optimal warming (or cooling) when tidal truncation leads to extended periods of low water depth ($h_r = h_{\min}$). Alternatively, we can consider the hypothetical case where offshore mean sea level is sufficiently high enough that tidal truncation does not occur (i.e., the reef platform becomes too deep at low tide); for this example, h_{MSL}^* is increased to $h_{\min}^* + 1 = 1.17$ so that the low tide depth is exactly equal to the minimum depth of $h_{\min}$ = 0.5 m (or $h_{\min}^* = 0.17$) for Tallon (Figure 25b). For this alternate case, the maximum dimensionless temperature fluctuations are substantially reduced ($\Delta T_r^* \approx 0.5$), with the maximum warming / cooling for this case instead occurring earlier in the tidal cycle, or when $\Delta\phi_i \approx 120°$. In other words, the combination of a symmetric tidal variation (with reduced low tide duration) and deeper water column leads to much lower temperature variations for a given maximum net heat flux $Q_{net,max}$ and tidal amplitude η_{tide}.

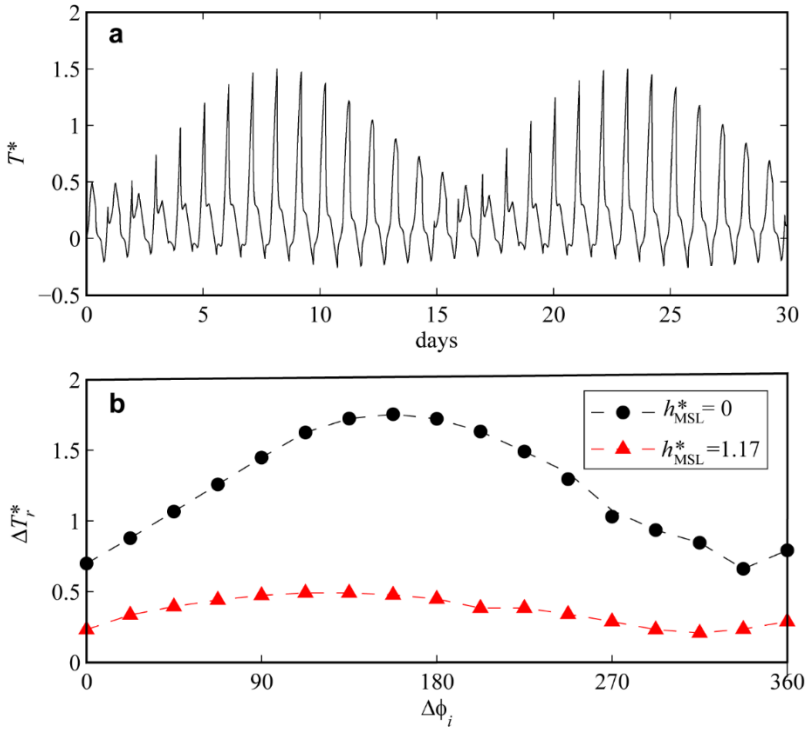

Figure 25. Response of reef temperature to interacting light and tidal cycles. (a) Reef temperature variability (in dimensionless form T_r^* per Eq. (21)) over 30 days, for an idealized Tallon reef ($h_{MSL}^* = 0$ and $h_{\min}^* = 0.17$), illustrating the 14.8 day modulation of the temperature fluctuations caused by the phase drift between the maximum tidal elevation and solar irradiance. (b) The maximum diurnal temperature variation ΔT_r^* (defined as the difference between the daily maximum and minimum value of T_r^*), as a function of the instantaneous phase difference between the tidal and solar cycle ($\Delta\phi_i$). Results shown are for an idealized Tallon reef under present-day sea level ($h_{MSL}^* = 0$) shown in (a), as well as a hypothetical scenario where mean sea level is increased so that the depth at low tide is equal to h_{min} (equivalent to $h_{MSL}^* = 1.17$) and tidal truncation no longer occurs.

Label	Site	η_{tide} (m)	F_{tide}	ΔT_r (% change)		ΔT_r (range, °C)			Reference
				MSL +0.7 m	MSL +1.5 m	present	MSL +0.7 m	MSL +1.5 m	
Ⓐ	Tallon Island, Kimberley, northwestern Australia	3.0	0.13	-7%	-18%	2.5-6.5	2.3-6.0	2.0-5.3	This study
Ⓑ	Warraber Island, Torres Straight	1.2	0.46	-23%	-72%	2.0-5.0	1.5-3.8	0.6-1.4	(Kench & Brander 2006)
Ⓒ	Cocos (Keeling) Islands, eastern Indian Ocean	0.6	0.48	-65%	-86%	NA	NA	NA	(Smithers & Woodroffe 2000)
Ⓓ	Lady Eliot, Great Barrier Reef	0.8	0.42	-39%	-78%	2.5-5.5	1.5-3.3	0.5-1.2	(McCabe et al. 2010, Shaw et al. 2012)
-	Ofu, American Samoa	0.5	0.15	-36%	-62%	1.5-6.0	1.0-3.8	0.6-2.3	(Craig et al. 2001)
-	Rarotonga, Cook Islands	0.4	0.16	-38%	-63%	NA	NA	NA	(Goodwin & Harvey 2008)

Table 4. Tidal amplitudes (η_{tide}) represent average values (i.e., intermediate between spring and neap). F_{tide} denotes the tidal form factor (see text for details). Diurnal temperature range changes (% ΔT_r change) are relative to present conditions with 0 m MSL. Present temperature ranges (ΔT_r) are drawn from literature values and projected for different mean sea level rise scenarios (+0.7 m and +1.5 m) using the model.

3.5.3 General influence of sea level rise on reef temperature extremes

We further apply the model over a realistic range of reef depths and tidal amplitudes to more generally assess how tides, surface heat fluxes and reef morphology interact to drive reef temperature variability across a broader range of reef morphologies and tidal amplitudes. Using this more global model, we then assess the sensitivity of the diurnal temperature extremes to sea level rise for a number of other reef systems from across the Indo-Pacific region. We consider six example reefs that have both detailed tidal records and accurately-surveyed reef profile bathymetry relative to mean sea level; thus providing us with robust estimates of both h^*_{MSL} and $h^*_{\min}$ (Tables 3 and 4). Fortunately, four of these six reefs also have detailed temperature data showing diurnal temperature extremes ranging from 1.5-6.5°C depending on the reef morphology, local tidal amplitude, time of year and weather conditions (Table 4). In particular, we investigate how maximum diurnal temperature fluctuations (in dimensionless form ΔT^*_r) over the 14.8 day cycle respond to variations in the

dimensionless reef depth parameters h^*_{MSL} and $h^*_{\min}$ (Eq. (21)). Prior analyses have shown that tidal truncation occurs only when the depth of the reef falls below a common physical boundary of $h^*_{MSL} \le h^*_{\min} + 1$ (Lowe et al. 2015), or in dimensional terms, when $h_{MSL} \le h_{\min} + \eta_{tide}$. The tidal-thermodynamic model reveals that ΔT^*_r increases when either h^*_{MSL} and/or $h^*_{\min}$ is decreased. This is mainly due to the net incident heat flux being distributed over a shallower water column (Figure 26). However, we further note that there is a very abrupt increase in ΔT^*_r when $h^*_{MSL} < h^*_{\min} + 1$ (i.e., when tidal truncation occurs). This is due to tidal truncation extending the duration of low water depths on the reef, thus elongating periods of enhanced heating / cooling of the shallow water column, and as a consequence, making the response of diurnal temperature variability to a changing sea level highly nonlinear.

To assess how sea level rise will specifically affect temperature extremes within each of these reef environments, we assume that both future tidal conditions and $Q_{net,max}$ remain unchanged. The former is determined solely by celestial mechanics while the latter is reasonable given that, with the exception of potential regional changes in cloud cover and decadal changes in solar radiation, $Q_{net,max}$ should remain relatively constant. Two sea level rise scenarios are considered based on predicted end of the century scenarios (see Methods): a 0.7 m rise based on IPCC projections from CMIP5 (Church et al. 2013) and a 1.5 m rise that captures the upper end of semi-empirical projections (see summary by Nicholls et al. 2011). In both cases, these rates of sea level rise far exceed typical reef accretion rates (Quataert et al. 2015). One very important aspect of our simple tidally-driven heat exchange model is that if $Q_{net,max}$ is kept constant (albeit approximately so), then the ratio of a given temperature extreme (ΔT_r) following sea level rise to present day values is independent of the particular local value of $Q_{net,max}$, due to the linear form of governing differential equation (Eq. (17)). Thus, although detailed in situ measurements of $Q_{net,max}$ may not be available for most reef sites, this data is not actually necessary for predicting how much temperature extremes at a given reef site will change as a consequence of sea level rise on a percentage basis.

The results indicate that 0.7 m of sea level rise would reduce present maximum diurnal temperature ranges (ΔT_r) by between 7-65% across the six reef sites while 1.5 m of sea level rise would reduce ΔT_r by 18-86% (Table 4). Reefs that already experience moderate tidal truncation now (i.e., where the offshore low tidal elevation falls just below the minimum depth) will experience the most substantial reductions in temperatures under future sea level rise. Such examples of reef systems near the 'tipping point' include Lady Elliot in the Great Barrier Reef and the Cocos Islands in the eastern Indian Ocean (Figure 26). Thus for reefs such as Lady Elliot where ΔT_r typically ranges from 2.5-5.5 ^{o}C at present, these extremes are predicted to be reduced to 1.5-3.3 ^{o}C under 0.7 m of sea level rise and to just 0.5-1.2 ^{o}C under 1.5 m of sea level rise.

A more general consequence of these results is how diurnal temperature extremes within different types of reefs worldwide will be affected by a rise in mean sea level depending on their mean depth and regionally-specific tidal amplitudes. From Figure 26a it is clear that those reefs presently located in a regime near the cusp of tidal truncation (i.e. those reefs with $h^*_{MSL} \approx h^*_{\min} + 1$) will experience the most substantial reductions in temperature extremes under future sea level rise due to the abrupt transition in ΔT^*_r that occurs when h_{MSL} becomes deeper than $h_{\min} + \eta_{tide}$ and tidal truncation ceases, as illustrated in Figure 26b. Given that many coral reef crests are presently located near mean sea level (Falter et al. 2013), it is very common for the offshore sea level to fall below the elevation of many reefs at low tide, and hence experience some form of

tidal truncation regardless of the regional tidal amplitude.

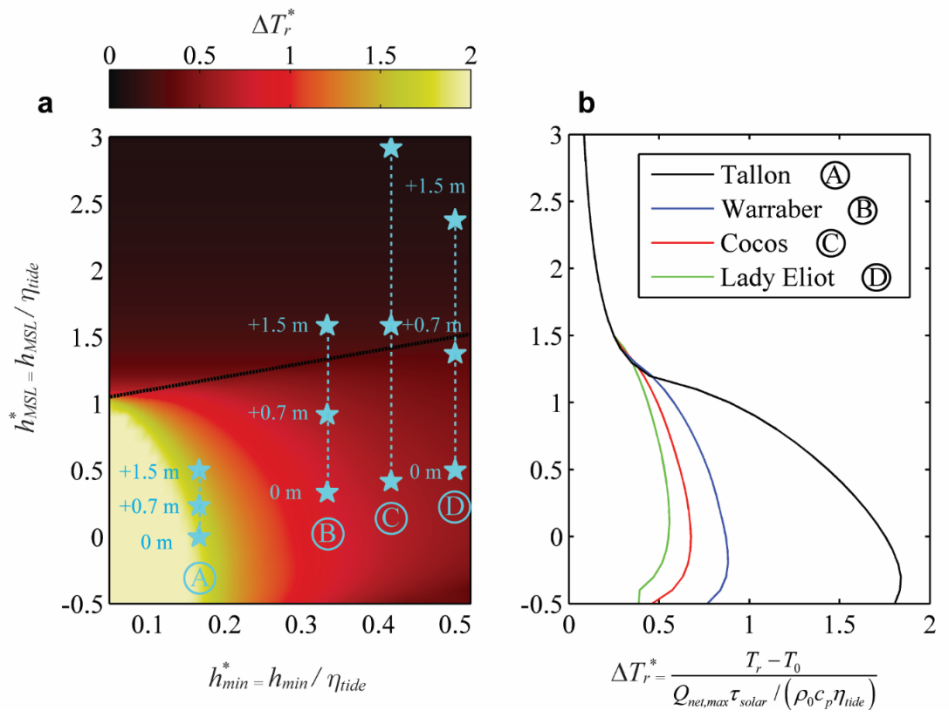

Figure 26. Diurnal temperature extremes for various reefs worldwide and their response to sea level rise. (a) The magnitude of the maximum diurnal temperature fluctuation (in dimensionless form), as a function of the normalized minimum reef water depth ($h^*_{\min}$) and normalized reef depth relative to mean sea level (h^*_{MSL}). Tidal truncation occurs below the black dotted line ($h^*_{MSL} \approx h^*_{\min} + 1$). The location of four reefs within this parameter space (A-D, see Tables 3 and 4) are shown for three mean sea level scenarios (0 m relative to present; a future +0.7 m rise; a future +1.5 m rise). Ⓐ = Tallon island, Ⓑ = Warraber island, Ⓒ = Cocos Islands, Ⓓ = Lady Elliot island. (b) The response of ΔT_r^* for the four reefs with fixed $h^*_{\min}$ but varying h^*_{MSL} .

4 Discussion and Conclusions

4.1 Observed water quality patterns and variability

4.1.1 Temperature and dissolved oxygen

Environmental conditions measured in this study easily rank among the most extreme recorded for reef systems worldwide (Kleypas et al. 1999). When low water depths occurred near midday, temperatures on the reef platform reached in excess of 36°C and showed high variability (in some cases >10°C) over a single day (Figure 13d). Extreme reef temperatures (>36°C) have been previously documented in the Red Sea and Arabian Gulf (Coles & Fadlallah 1991, Ateweberhan et al. 2006), and diel fluctuations of ~8°C can occur in the Gulf of Oman (Coles 1997) and shallow backreef environments such as Ofu, American Samoa (Craig et al. 2001) or One Tree Island, Australia (Silverman et al. 2012). Similar patterns have also been recorded in some seagrass studies, as the species present on Tallon reef (*E. acoroides* and *T. hemprichii*) often occur in intertidal environments that can experience elevated temperatures (>35°) on sub-daily timescales (Bridges & McMillan 1986, Collier & Waycott 2014).

This study documented extremes in DO saturation on sub-daily timescales, where supersaturation (up to 280%) occurred with midday low water levels and up to 7.5 hours of hypoxia occurred at night (Figure 13c). Similar ranges in DO have been recorded in shallow backreef areas (Piniak & Brown 2009, Koweek et al. 2015b) and

lagoon waters isolated during semidiurnal low tides (Silverman et al. 2012) or spring low tides (Ohde & van Woesik 1999). Hypoxia is known to occur in the diffusive boundary layer around reef organisms and in organism tissue (Kühl et al. 1995, Ulstrup et al. 2005, Pedersen et al. 2016), but is not typically reported in reef water columns, with very few exceptions (Koweek et al. 2015b) and not to the extent of Tallon reef. The length of both field studies presented here allowed capture of water quality over nearly the full set of tide/light interactions (~14.8 days) (Lowe et al. 2016). Although temperature and DO extremes over the year undoubtedly exceed what is presented here, these water quality patterns can nonetheless be considered representative for this reef.

4.1.1 Dissolved nutrients and chlorophyll

Nutrient and chlorophyll-*a* concentrations showed strong patterns associated with tidal flooding on the reef platform. The chlorophyll-*a* signal seen in daily time-series indicated the importance of twice-daily tidal inundation for replenishing labile algal and detrital material for reef filter-feeders.

Overall, Tallon reef was found to be oligotrophic (low dissolved nutrients and chl-*a*), which is normal for tropical waters that do not receive substantial anthropogenic nutrient loads from terrestrial runoff. Nutrient loading negatively impacts coral health in several ways (Szmant 2002, Fabricius 2005), and is one of many stressors causing coral decline in reefs worldwide. Large rainfall events, such as the monsoon or tropical cyclones, cause pulses of nutrients to enter coastal waters; these nutrient delivery events have received much attention in the Great Barrier Reef Marine Park (Devlin & Brodie 2005, Devlin & Schaffelke 2009, Kroon et al. 2012), and hundreds of millions of dollars have already been spent in attempts to ameliorate water quality.

The statistically significant increase in DIN (more than doubled) and chl-*a* measured through the wet season period (Figure 23) indicated that wet season terrestrial discharge did reach the Sunday Island reef group, although it may have been substantially transformed and remineralised along the way. The fact that a measureable change in nutrients occurred was surprising given the strong mixing, both vertically and between King Sound and offshore waters. Additionally, the 2013/2014 Wet season had low rainfall levels relative to wet seasons from the previous 18 years (Figure 27). Higher rainfall would very likely result in larger pulses of labile terrestrial material to King Sound than what was measured here. A great deal more research is necessary before we can understand how coastal water quality is affected by the wet season in the Kimberley region.

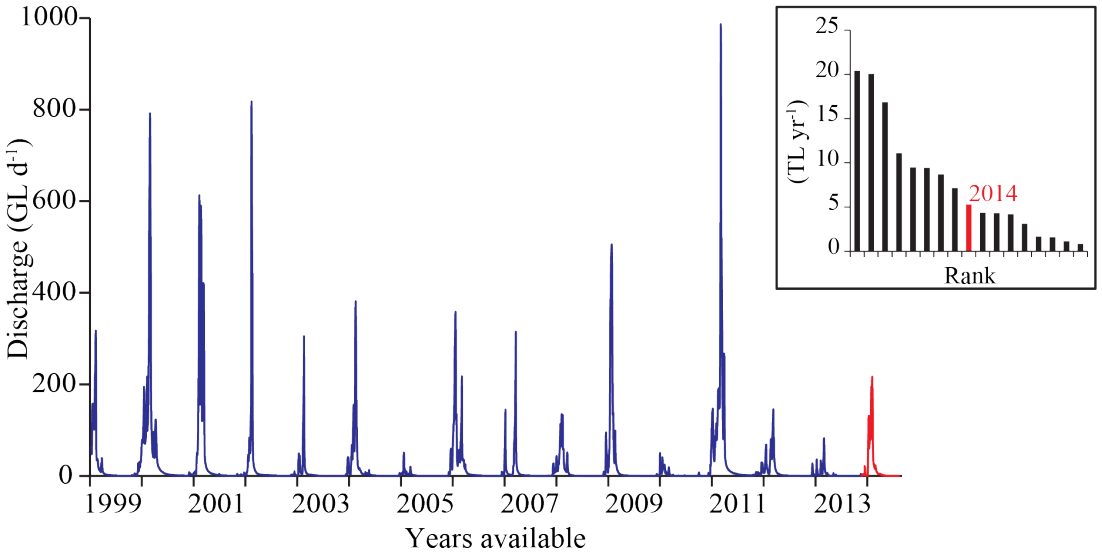

Figure 27. Fitzroy River discharge measured at Willare (site 802008 Dept. of Water) from 1998 – 2014. Upper right inset shows years ranked by annual discharge, with 2013/2014 Wet season highlighted in red.

4.2 Productivity and respiration

4.2.1 Components of benthic oxygen flux

The use of a one-dimensional control volume approach in this study allowed estimation of rates of community production at high frequency (half-hourly) during ebb tides by accounting for changes in oxygen due to local accumulation, cross-reef advection, and air-sea gas transfer. The local component dominated in both communities (Figure 14), likely due to the dense biomass of primary producers, the shallow water depth, and slow flow (<5 cm s^{-1}) during large portions of ebb tide.

The advective component was relatively larger in the macroalgal community compared to the seagrass community. This was likely partially due to the location of loggers relative to community boundaries; water that entered the macroalgal control volume (advected past RDO2) had previously overlain a different and less productive community (seagrass), which led to an oxygen concentration gradient between RDO2 and RDO3. Whereas, water that entered the seagrass control volume (advected past RDO1) had previously overlain similar seagrass community, and thus a strong oxygen concentration gradient did not develop between RDO1 and RDO2. This result suggests that reef flat metabolism on similar high intertidal reefs (Solihuddin et al. 2016) may be estimated for portions of the tidal cycle using Eulerian methods alone provided flow patterns are well-established, the community of interest is of sufficient size, and sensor positions relative to community boundaries are carefully considered. For other tide-dominated reefs where flow speeds remain moderate throughout the tidal cycle (e.g., ≥ 5 cm s^{-1}) and transit times are short, advective components may comprise a large proportion of J_{O2} (Falter et al. 2012).

The air-sea gas flux was a relatively minor component (<10%) of diel oxygen patterns in both communities (Figure 14), which is typical of reef systems (Frankignoulle et al. 1996). As this reef flat was characterised by shallow water depths (during J_{O2} estimation), negligible wave action, low wind speeds (~3 m s^{-1}, Table 1), and variable flow speeds, a parameterization of air-sea gas flux for turbulent open-channel flow (Chu & Jirka 2003) was deemed more appropriate than those from high wave and wind conditions commonly-used in reef studies (Wanninkhof 1992, Ho et al. 2006). The minor contribution of air-sea gas flux to J_{O2} estimates despite diel extremes in oxygen saturation was surprising, but was likely due to the coincidence of low flow (Figure 13), and thus small k_{O2}, with these saturation extremes.

4.2.1 Patterns in hourly community respiration

Estimates of nighttime community respiration in this study showed large variability expressed in a regular pattern with diel and tidal cycles. When nighttime coincided fully with ebb tide, rates of CR_{dark} were greatest directly after sunset and declined steadily through the night (Figure 14C). Similar patterns have been documented in previous studies and are generally attributed to declines in internal dissolved organic carbon stores (photosynthates) of benthic organisms (Falter et al. 2011, Silverman et al. 2012, Long et al. 2013). In our study, these changes could be due to: 1) declines in nighttime temperatures from air-sea heat exchange, 2) changes in flow speed over ebb tide, 3) changes in oxygen concentration, or 4) DOC (photosynthate) limitation in benthic organisms. Each explanation is discussed in detail below.

The wide range of environmental conditions on Tallon Island reef and large number of observations resulted in CR_{dark} estimates from a broad range of temperature (28.5 – 32.5°C), DO (7 – 300 μM), and flow speed (0.01 – 0.20 m s^{-1}). Falling nighttime temperatures due to air-sea heat flux explained merely ~8% of the diel pattern in CR_{dark}. Uptake rate coefficients for CR_{dark} did not increase with u_x, indicating that CR_{dark} was not controlled by flow speed with the exception of low flows where it approached mass transfer limitation (Figure 15). We found strong trends between CR_{dark} and DO concentration (Figure 16), which potentially indicate that CR_{dark} was DO-limited by low DO and stimulated by high DO. These relationships did not change when only the first two hours after sunset were used, which suggests that internal DOC limitation was not involved in CR_{dark} patterns. The dependence of CR_{dark} on DO concentration has been shown in a few previous studies, either as a Monod-type saturating (Zimmerman et al. 1989) or linear (Atkinson et al. 1994) relationship. This is an important finding

because it helps us understand controls on daytime community respiration (which cannot be estimated directly) and allows us to more rigorously estimate gross primary production. It also helps us to better predict the effects of climate change and other future stressors of Kimberley reefs based on an understanding of which environmental conditions most affect metabolism.

Daytime community respiration is commonly estimated in metabolism studies as the constant mean of CR_{dark} (Long et al. 2013). We believe that for this reef (and other Kimberley reefs experiencing large diel swings in oxygen), CR_{light} can be represented as a function of DO and is therefore generally high during the daytime. A small number of studies show that daytime respiration of reef organisms exceeds that of nighttime (Kühl et al. 1995), but much more research is necessary. This finding is important in the context of the following sub-section.

4.2.2 Diurnal variations in hourly production

Hysteresis in photosynthesis-irradiance curves (declines in NP in the afternoon relative to NP in the morning, Figure 17) is often seen in seagrass and reef metabolism studies (Long et al. 2013, Koweek et al. 2015a, Adams et al. 2016) and is attributed to many different things, including high light/temperature inhibition of photosynthesis, or light history-dependent respiration. In this study, we have shown that elevation of CR_{light} due to high afternoon DO levels most likely caused hysteresis in NP at upper irradiances.

When gross primary production of reef platform communities was estimated accounting for increases in CR_{light}, hysteresis in production rates was not evident in either community (Figure 18). Thus, seagrass and macroalgal communities were able to maintain high rates of photosynthetic carbon fixation across a wide range of temperatures and high irradiance. *Thalassia hemprichii* is an intertidal species that has previously been documented in environments with short term temperature increases to ~35°C (McMillan 1984, Campbell et al. 2006, Collier & Waycott 2014, Pedersen et al. 2016). Despite periods of high temperature, small coral thrived on the reef platform; research suggests that water flow and thermal acclimation (Nakamura & Van Woesik 2001, Nakamura et al. 2003) may mitigate coral bleaching when temperatures are elevated. Regardless, this finding illustrates that Kimberley reef platform communities are well-adapted to short-term exposures to high temperature/light and expands our understanding of reef community tolerance to stressors.

4.2.3 Metabolism over daily to weekly time-scales

Rates of daily GPP and CR from the macroalgal community (700 and 670 mmol O_2 m^{-2} d^{-1}, respectively) were within the range of estimates from most reef systems from across the Indo-Pacific (300-1300 mmol O_2 m^{-2} d^{-1}) (Falter et al. 2013), and similar to mean values for reef flats (740 and 640 mmol O_2 m^{-2} d^{-1}, respectively). Rates of GPP and CR for the seagrass community (490 and 440 mmol O_2 m^{-2} d^{-1}, respectively) were well above the global mean for tropical seagrass systems (252 and 217 mmol O_2 m^{-2} d^{-1}, respectively) (Duarte et al. 2010). At the reef scale, our study estimated daily metabolism similar to the mean of previous studies, despite the extreme conditions present (Figure 28). The production to respiration ratio estimated in our study (1.0) was slightly less than the mean of Indo-Pacific reefs (1.24). The P:R ratio estimated for seagrasses (1.1) was slightly lower than the mean of 1.61 from tropical seagrass studies (Duarte et al. 2010). The balanced P:R ratios of Tallon Island reef communities indicate that the reef is neither a net source nor sink of carbon to adjacent systems.

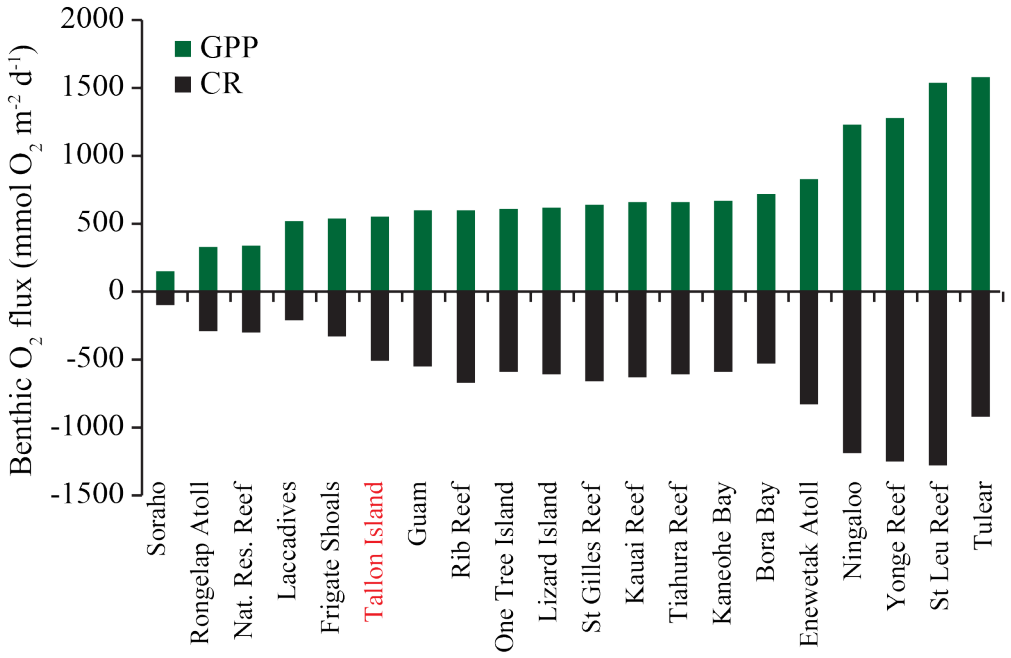

Figure 28. Comparison of daily rates of gross primary production and community respiration of Tallon Island (highlighted red) with other reef productivity studies from the Indo-Pacific region from (Falter et al. 2013).

One of the most interesting findings from this study was the relationship between daily net community production and the light-tide phase difference (Figure 19), which has cycles of ~15 day length (the same as for temperature in section 3.5.2). This shows that the reef platform varies between net autotrophic and net heterotrophic depending on location within this ~15 day envelope. The oscillation between positive and negative NCP is likely driven by the time of day when low water depths occur. For example, low water depth during sunrise/sunset (~0°), would result in high NCP due to low rates of CR (low temperatures and DO). Conversely, low water depth during ~noon/midnight (~180°) would result in low NCP due to high rates of CR. Many productivity studies last only a few days, which could lead to large overestimates in net production if the study occurred ~0° phase difference or large underestimates if the study occurred ~180° phase difference. This finding suggests that metabolism or other biogeochemical studies should be conducted over a ~2 week period to gain a representative estimate of the biogeochemical process of interest. Additionally, point measurements of temperature, oxygen, nutrients, and other water quality variables on Kimberley reefs will have little ecological relevance without a physical context.

In summary, this study demonstrated that Tallon reef is a moderately productive and metabolically balanced system thriving in some of the most extreme environmental conditions measured worldwide. Through use of the one-dimensional control volume method, we were able to estimate metabolism over a natural range of conditions that would be very difficult to replicate in the laboratory. Relationships between reef metabolism and environmental variables determined in this study can most likely be extended to other Kimberley reefs that experience periods of low water depth. We found that reef gross primary productivity was not affected by high temperature in the short-term, most likely because communities are well-adapted to extreme diel variations. The reef communities varied between net autotrophic and net heterotrophic depending on the interaction between tidal and solar cycles. Our study shows that a strong understanding of reef hydrodynamics is necessary to interpret measurements of temperature, oxygen, and nutrient levels on Kimberley reefs. The estimates of metabolism and key environmental drivers presented here give us a basis to understand reef response to future stressors.

4.3 Physical drivers of extreme temperature and water quality variability in tide-dominated reefs

The results demonstrate how the phase differences between solar heating and tidal cycles can drive variability in temperature extremes within the Kimberley's reefs, whose amplitude oscillates over a ~14.8 day period as a result of differences between Earth's rotational and moon's orbital period. The present study focused specifically on the interaction associated with the principal lunar semi-diurnal (M2) tidal constituent that tends to be the dominant constituent in most locations globally, particularly in the tropics. While other tidal constituents with different frequencies can similarly induce different frequency interactions, the general framework and model described here can be readily extended to investigate other tidal scenarios, including under mixed (semi-diurnal + diurnal) conditions. For the generally dominant M2 constituent considered here, the interaction between the different tidal and solar forcing periods leads to a ~14.8 day modulation of the diurnal temperature fluctuations. We note that our results are similar to the ~14.8 day thermal cycle theorized and observed by Vugts (1975) within periodically drying tidal flats in estuaries; however, the physical mechanisms driving temperature variations in these estuarine systems are not the same as in the reef systems considered here. In Vugts (1975), the tidal modulation in the heat balances occurs via large tidal changes in the wetted surface area of shallow tidal flat systems (which alters air-sea heat exchange), with the response to heat advection being neglected over the large-scales considered in these studies (i.e., at scales larger than a tidal excursion length). However, most reef systems have well-defined shorelines bounded by sloping beaches, or in the case of Tallon Island rocky coastal topography, that results in only minimal changes in reef surface area over a tidal cycle. Instead, tidally-driven advection drives substantial heat exchange between a reef and the ocean, which plays a dominant role in the tidal modulation of these reef heat balances by modifying reef water residence times.

The particular morphology of a reef also plays a very important role in regulating temperature variability. As a consequence, tidal variability over tide-dominated reefs is frequently asymmetric, with longer fall durations than rise durations (Ludington 1979, Wilson 1985, Callaghan et al. 2006, McCabe et al. 2010, Lowe et al. 2015). This effect of tidal truncation arises from the restriction of water draining out of a reef, either by bottom friction or topographic constraints such as a shallower crest (Lowe et al. 2015), which can have a very important influence on the magnitude of diurnal reef temperature variations. Such tidal asymmetry acts to extend the low tide period when shallow water persists on a reef, thereby enhancing daytime warming (or night time cooling). This not only substantially increases the magnitude of diurnal temperature extremes, but also the phase difference between the solar and tidal cycle when these maximum temperatures occur.

An important implication of these results is how sea level rise could alter reef heat balances in the future, and hence, may partially contribute to limiting local reef temperature extremes in the presence of a globally warming ocean. It may seem intuitive, at first, that reefs with large tidal exposure would be less sensitive to sea level changes, given that the degree of mean sea level change will be comparatively smaller than natural sea level variations these reefs already experience on a daily basis. However, in terms of diurnal temperature variability, our results indicate that reefs subject to large tidal amplitudes can be affected just as much by a sea level rise as those subject to small tidal amplitudes (Figure 26a). Reefs that are already close to the critical depth at which tidal truncation ceases (i.e., near $h_0^* = h_{\min}^* + 1$) are particularly close to a 'tipping point' where even a relatively small increase in mean sea level can lead to a substantial reduction in the magnitude of diurnal temperature fluctuations. In some cases, reefs that presently experience +5^{o}C diurnal temperature extremes could see a >2 ^{o}C reduction in these temperatures from a 0.7 m sea level rise, or a >4 ^{o}C reduction by a 1.5 m rise (Table 4); amounts that are comparable in magnitude to projected warming of the tropical oceans by the end of the century under a business-as-usual scenario (2-4°C, Bopp et al. (2013)). It is not yet known, however, how much future reductions in local temperature variability will ameliorate the more chronic thermal stresses imposed by long-term increases in regional ocean temperature.

Finally, while the focus of this study has been on the temperature extremes of tide-dominated reefs, the results are also relevant to understanding the role of tides on many other reef water quality parameters. For example,

changes in reef water column oxygen, pCO_2, and pH are also governed just as much by the morphology of the reef and the hydrodynamic forces driving circulation as they are by the fluxes driving their non-conservative behavior (Falter et al. 2013). Furthermore, the specific processes responsible for driving changes in oxygen, *p*CO2, and pH (i.e., production, respiration, and net calcification) also exhibit light-dependent diurnal periodicities similar to the net atmospheric heat fluxes used in the present model, albeit with much greater spatial variation in the biologically-driven bottom boundary fluxes (Lowe & Falter 2015). Thus, we expect sea level rise to also cause reductions in daily extremes of oxygen, pCO_2, and pH in similar proportion to the reductions in daily temperature extremes that we report here. Although there is little doubt that rising levels of atmospheric pCO_2 will cause substantial changes to ocean temperature and chemistry over the following century, we conclude that rising sea levels will likely help moderate the extreme conditions presently found in many shallow, tide-dominated reef habitats.

4.4 Recommendations for future work

The project has provided a reasonably complete assessment of how environmental variability, including temperature, light, oxygen and water motion, influence the productivity of benthic communities in the Kimberley. Due to the process-focused nature of the experiments, we expect the general relationships and models developed in this project to be extended to other reef systems with some confidence. In other words, if the environmental conditions and habitat characteristics of other reefs in the Kimberley are known, or can be reasonably predicted, we believe the robust estimates of the productivity of other reefs in the Kimberley can be made.

Therefore, a natural future step will be to integrate future information about reef characteristics across the broader Kimberley region, including properties of reef morphology, habitats and benthic community structure. While beyond the scope of the present project, this will enable our results to be extended more broadly across the Kimberley to, for example, obtain quantitative estimates and maps of reef productivity across the region.

Further work is also needed to develop a more comprehensive view of nutrient dynamics for reefs in the Kimberley. Given the intensive nature of the two year field program, which happened to focus on the 2013-14 period that was unusually dry, future work should compare these observations to more typical wet seasons. While the results from this study did not indicate any substantial differences in reef nutrient dynamics between seasons, this may not always be the case, particularly during anomalously wet years. To understand this inter-annual variability, future research would benefit from regular water quality monitoring across the coastal Kimberley.

5 References

Adams MP, Ferguson AJP, Maxwell PS, Lawson BAJ, Samper-Villarreal J, O'Brien KR (2016) Light history-dependent respiration explains the hysteresis in the daily ecosystem metabolism of seagrass. Hydrobiologia 766:75-88

Ateweberhan M, Bruggemann JH, Breeman AM (2006) Effects of extreme seasonality on community structure and functional group dynamics of coral reef algae in the southern Red Sea (Eritrea). Coral Reefs 25:391-406

Atkinson M, Kotler E, Newton P (1994) Effects of water velocity on respiration, calcification, and ammonium uptake of a *Porites compressa* community.

Berry JA, Raison JK (1981) Responses of macrophytes to temperature. Physiological Plant Ecology I. Springer Berlin Heidelberg

Bopp L, Resplandy L, Orr JC, Doney SC, Dunne JP, Gehlen M, Halloran P, Heinze C, Ilyina T, Séférian R (2013) Multiple stressors of ocean ecosystems in the 21st century: projections with CMIP5 models. Biogeosciences 10:6225-6245

Borges AV, Delille B, Schiettecatte L-S, Gazeau F, Abril G, Frankignoulle M (2004) Gas transfer velocities of CO_2 in three European estuaries (Randers Fjord, Scheldt, and Thames). Limnol Oceanogr 49:1630-1641

Bridges KW, McMillan C (1986) The distribution of seagrasses of Yap, Micronesia, with relation to low tide conditions. Aquat Bot 24:403-407

Brocx M, Semeniuk V (2011) The global geoheritage significance of the Kimberley coast, Western Australia. J R Soc West Aust 94:57-88

Bryant D, Burke L, McManus J, Spalding M (1998) Reefs at risk: a map-based indicator of threats to the world's coral reefs. World Resources Institute, Washington, DC

Burd AB, Dunton K (2001) Field verification of a light-driven model of biomass changes in the seagrass *Halodule wrightii*. Mar Ecol Prog Ser 209:85-98

Callaghan DP, Nielsen P, Cartwright N, Gourlay MR, Baldock TE (2006) Atoll lagoon flushing forced by waves. Coast Eng 53:691-704

Campbell SJ, McKenzie LJ, Kerville SP (2006) Photosynthetic responses of seven tropical seagrasses to elevated seawater temperature. J Exp Mar Biol Ecol 330:455-468

Chu CR, Jirka GH (2003) Wind and stream flow induced reaeration. J Environ Sci (Mount Prospect, Ill) 129:1129-1136

Church JA, Clark PU, Cazenave A, Gregory JM, Jevrejeva S, Levermann A, Merrifield M, Milne G, Nerem R, Nunn P (2013) Sea level change. In: Stocker T, Qin D, Plattner G, Tignor M, Allen S, Boschung J, Nauels A, Xia Y, Bex V, Midgley P (eds) Climate Change 2013: The Physical Science Basis Contribution of Working Group I to the Fifth Assessment Report of the Intergovernmental Panel on Climate Change. Cambridge University Press

Cole JJ, Pace ML, Carpenter SR, Kitchell JF (2000) Persistence of net heterotrophy in lakes during nutrient addition and food web manipulations. Limnol Oceanogr 45:1718-1730

Coles LS (1997) Reef corals occurring in a highly fluctuating temperature environment at Fahal Island, Gulf of Oman (Indian Ocean). Coral Reefs 16:269-272

Coles SL, Fadlallah YH (1991) Reef coral survival and mortality at low temperatures in the Arabian Gulf: New species-specific lower temperature limits. Coral Reefs 9:231-237

Collier CJ, Waycott M (2014) Temperature extremes reduce seagrass growth and induce mortality. Mar Pollut Bull 83:483-490

Collins LB, O'Leary M, Stevens A, Bufarale G, Kordi M, Solihuddin T (2015) Geomorphic patterns, internal architecture and reef growth in a macrotidal, high-turbidity setting of coral reefs from the Kimberley bioregion. Australian Journal of Maritime & Ocean Affairs 7:12-22

Craig P, Birkeland C, Belliveau S (2001) High temperatures tolerated by a diverse assemblage of shallow-water corals in American Samoa. Coral Reefs 20:185-189

Crossland C, Hatcher B, Smith S (1991) Role of coral reefs in global ocean production. Coral Reefs 10:55-64

Davis KA, Lentz SJ, Pineda J, Farrar JT, Starczak VR, Churchill JH (2011) Observations of the thermal environment on Red Sea platform reefs: A heat budget analysis. Coral Reefs 30:25-36

Devlin M, Schaffelke B (2009) Spatial extent of riverine flood plumes and exposure of marine ecosystems in the Tully coastal region, Great Barrier Reef. Aust J Mar Freshwater Res 60:1109-1122

Devlin MJ, Brodie J (2005) Terrestrial discharge into the Great Barrier Reef Lagoon: nutrient behavior in coastal waters. Mar Pollut Bull 51:9-22

Duarte CM, Marbà N, Gacia E, Fourqurean JW, Beggins J, Barrón C, Apostolaki ET (2010) Seagrass community metabolism: Assessing the carbon sink capacity of seagrass meadows. Global Biogeochemical Cycles 24

Fabricius KE (2005) Effects of terrestrial runoff on the ecology of corals and coral reefs: review and synthesis. Mar Pollut Bull 50:125-146

Fairall CW, Bradley EF, Hare JE, Grachev AA, Edson JB (2003) Bulk parameterization of air–sea fluxes: Updates and verification for the COARE algorithm. J Clim 16:571-591

Falter JL, Atkinson MJ, Merrifield MA (2004) Mass-transfer limitation of nutrient uptake by a wave-dominated reef flat community. Limnol Oceanogr 49:1820-1831

Falter JL, Atkinson MJ, Schar DW, Lowe RJ, Monismith SG (2011) Short-term coherency between gross primary production and community respiration in an algal-dominated reef flat. Coral Reefs 30:53-58

Falter JL, Lowe RJ, Atkinson MJ, Cuet P (2012) Seasonal coupling and de-coupling of net calcification rates from coral reef metabolism and carbonate chemistry at Ningaloo Reef, Western Australia. J Geophys Res Oceans 117:C05003

Falter JL, Lowe RJ, Zhang Z, McCulloch M (2013) Physical and biological controls on the carbonate chemistry of coral reef waters: Effects of metabolism, wave forcing, sea level, and geomorphology. PLoS ONE 8:e53303

Frankignoulle M, Gattuso J, Biondo R, Bourge I, Copin-Montégut G, Pichon M (1996) Carbon fluxes in coral reefs. II. Eulerian study of inorganic carbon dynamics and measurement of air-sea CO_2 exchanges. Mar Ecol Prog Ser 145:123-132

Goodwin ID, Harvey N (2008) Subtropical sea-level history from coral microatolls in the Southern Cook Islands, since 300 AD. Mar Geol 253:14-25

Halpern BS, Walbridge S, Selkoe KA, Kappel CV, Micheli F, D'Agrosa C, Bruno JF, Casey KS, Ebert C, Fox HE, Fujita R, Heinemann D, Lenihan HS, Madin EMP, Perry MT, Selig ER, Spalding M, Steneck R, Watson R (2008) A global map of human impact on marine ecosystems. Science 319:948-952

Ho DT, Law CS, Smith MJ, Schlosser P, Harvey M, Hill P (2006) Measurements of air-sea gas exchange at high wind speeds in the Southern Ocean: Implications for global parameterizations. Geophys Res Lett 33:L16611

Horstman M, Wightman G (2001) Karparti ecology: Recognition of Aboriginal ecological knowledge and its application to management in north-western Australia. Ecol Manage Restor 2:99-109

Jassby AD, Platt T (1976) Mathematical formulation of the relationship between photosynthesis and light for phytoplankton. Limnol Oceanogr 21:540-547

Kench PS, Brander RW (2006) Wave processes on coral reef flats: Implications for reef geomorphology using Australian case studies. J Coast Res:209-223

Kleypas JA, McManus JW, Meñez LAB (1999) Environmental limits to coral reef development: Where do we draw the line? Am Zool 39:146-159

Kowalik Z (2004) Tide distribution and tapping into tidal energy. Oceanologia 46:291-331

Koweek D, Dunbar RB, Rogers JS, Williams GJ, Price N, Mucciarone D, Teneva L (2015a) Environmental and ecological controls of coral community metabolism on Palmyra Atoll. Coral Reefs 34:339-351

Koweek DA, Dunbar RB, Monismith SG, Mucciarone DA, Woodson CB, Samuel L (2015b) High-resolution physical and biogeochemical variability from a shallow back reef on Ofu, American Samoa: An end-member perspective. Coral Reefs 34:979-991

Kroon FJ, Kuhnert PM, Henderson BL, Wilkinson SN, Kinsey-Henderson A, Abbott B, Brodie JE, Turner RDR (2012) River loads of suspended solids, nitrogen, phosphorus and herbicides delivered to the Great Barrier Reef lagoon. Mar Pollut Bull 65:167-181

Kühl M, Cohen Y, Dalsgaard T, Jorgensen BB, Revsbech NP (1995) Microenvironment and photosynthesis of zooxanthellae in scleractinian corals studied with microsensors for O_2, pH and light. Mar Ecol Prog Ser 117:159-172

Kundu P, Cohen LM (1990) Fluid Mechanics, Academic, Calif

Kvale EP (2006) The origin of neap–spring tidal cycles. Mar Geol 235:5-18

Lentz SJ, Churchill JH, Marquette C, Smith J (2013) Evaluation and recommendations for improving the accuracy of an inexpensive water temperature logger. J Atmos Ocean Technol 30:1576-1582

Long MH, Berg P, de Beer D, Zieman JC (2013) In situ coral reef oxygen metabolism: An eddy correlation study. PLoS ONE 8:e58581

Lowe RJ, Falter JL (2015) Oceanic forcing of coral reefs. Annu Rev Mar Sci 7:43-66

Lowe RJ, Leon AS, Symonds G, Falter JL, Gruber R (2015) The intertidal hydraulics of tide-dominated reef platforms. J Geophys Res Oceans 120:4845-4868

Lowe RJ, Pivan X, Falter J, Symonds G, Gruber R (2016) Rising sea levels will reduce extreme temperature variations in tide-dominated reef habitats. Sci Adv 2

Ludington C (1979) Tidal modifications and associated circulation in a platform reef lagoon. Aust J Mar Freshwater Res 30:425-430

McCabe RM, Estrade P, Middleton JH, Melville WK, Roughan M, Lenain L (2010) Temperature variability in a shallow, tidally isolated coral reef lagoon. J Geophys Res Oceans 115:C12011

McDonald C, Koseff J, Monismith S (2006) Effects of the depth to coral height ratio on drag coefficients for unidirectional flow over coral. Limnol Oceanogr 51:1294-1301

McGowan HA, Sturman AP, MacKellar MC, Wiebe AH, Neil DT (2010) Measurements of the local energy balance over a coral reef flat, Heron Island, southern Great Barrier Reef, Australia. J Geophys Res Atmos 115:D19124

McMillan C (1984) The distribution of tropical seagrasses with relation to their tolerance of high temperatures. Aquat Bot 19:369-379

Moberg F, Folke C (1999) Ecological goods and services of coral reef ecosystems. Ecol Econ 29:215-233

Monismith S (2007) Hydrodynamics of coral reefs. Annu Rev Fluid Mech 39:37-55

Nakamura T, Van Woesik R (2001) Water-flow rates and passive diffusion partially explain differential survival of corals during the 1998 bleaching event. Mar Ecol Prog Ser 212:301-304

Nakamura T, Yamasaki H, Van Woesik R (2003) Water flow facilitates recovery from bleaching in the coral *Stylophora pistillata*. Mar Ecol Prog Ser 256:287-291

Nicholls RJ, Marinova N, Lowe JA, Brown S, Vellinga P, De Gusmao D, Hinkel J, Tol RS (2011) Sea-level rise and its possible impacts given a 'beyond 4 C world'in the twenty-first century. Philosophical Transactions of the Royal Society of London A: Mathematical, Physical and Engineering Sciences 369:161-181

Odum HT, Odum EP (1955) Trophic structure and productivity of a windward coral reef community on Eniwetok Atoll. Ecol Monogr 25:291-320

Ohde S, van Woesik R (1999) Carbon dioxide flux and metabolic processes of a coral reef, Okinawa. Bull Mar Sci 65:559-576

Pedersen O, Colmer TD, Borum J, Zavala-Perez A, Kendrick GA (2016) Heat stress of two tropical seagrass species during low tides–impact on underwater net photosynthesis, dark respiration and diel in situ internal aeration. New Phytol 210:1207-1218

Piniak Ga, Brown EK (2009) Temporal variability in chlorophyll fluorescence of back-reef corals in Ofu, American Samoa. Biol Bull 216:55-67

Purcell S (2002) Intertidal reefs under extreme tidal flux in Buccaneer Archipelago, Western Australia. Coral Reefs 21:191-192

Quataert E, Storlazzi C, van Rooijen A, Cheriton O, van Dongeren A (2015) The influence of coral reefs and climate change on wave-driven flooding of tropical coastlines. Geophys Res Lett 42:6407-6415

Ramsing N, Gundersen J (1994) Seawater and gases. Tabulated physical parameters of interest to people working with microsensors in marine systems.

Shaw EC, McNeil BI, Tilbrook B (2012) Impacts of ocean acidification in naturally variable coral reef flat ecosystems. J Geophys Res Oceans 117:C03038

Silverman J, Kline DI, Johnson L, Rivlin T, Schneider K, Erez J, Lazar B, Caldeira K (2012) Carbon turnover rates in the One Tree Island reef: A 40-year perspective. J Geophys Res Biogeosci 117:G03023

Smithers SG, Woodroffe CD (2000) Microatolls as sea-level indicators on a mid-ocean atoll. Mar Geol 168:61-78

Solihuddin T, O'Leary MJ, Blakeway D, Parnum I, Kordi M, Collins LB (2016) Holocene reef evolution in a macrotidal setting: Buccaneer Archipelago, Kimberley Bioregion, Northwest Australia. Coral Reefs:1-12

Staehr PA, Testa JM, Kemp WM, Cole JJ, Sand-Jensen K, Smith SV (2012) The metabolism of aquatic ecosystems: History, applications, and future challenges. Aquat Sci 74:15-29

Szmant AM (2002) Nutrient enrichment on coral reefs: Is it a major cause of coral reef decline? Estuaries 25:743-766

Thomas FIM, Atkinson MJ (1997) Ammonium uptake by coral reefs: Effects of water velocity and surface roughness on mass transfer. Limnol Oceanogr 42:81-88

Ulstrup KE, Hill R, Ralph PJ (2005) Photosynthetic impact of hypoxia on in hospite zooxanthellae in the scleractinian coral *Pocillopora damicornis*. Mar Ecol Prog Ser 286:125-132

Valiela I (1995) Marine ecological processes. Springer-Verlag New York

Vugts H (1975) Interaction between the daily heat balance and the tidal cycle. Nature 255:113-117

Wanninkhof R (1992) Relationship between wind speed and gas exchange over the ocean. J Geophys Res Oceans 97:7373-7382

Weiss RF (1970) The solubility of nitrogen, oxygen and argon in water and seawater. Deep-Sea Res Oceanogr Abstr 17:721-735

Wells F, Hanley JR, Walker DI (1995) Marine biological survey of the southern Kimberley, Western Australia. Western Australian Museum

Wilson P (1985) Tidal studies in the One Tree Island lagoon. Aust J Mar Freshwater Res 36:139-156

Zappa CJ, Raymond PA, Terray EA, McGillis WR (2003) Variation in surface turbulence and the gas transfer velocity over a tidal cycle in a macro-tidal estuary. Estuaries 26:1401-1415

Zhang Z, Falter J, Lowe R, Ivey G, McCulloch M (2013) Atmospheric forcing intensifies the effects of regional ocean warming on reef-scale temperature anomalies during a coral bleaching event. J Geophys Res Oceans 118:4600-4616

Zimmerman RC, Smith RD, Alberte RS (1989) Thermal acclimation and whole-plant carbon balance in *Zostera marina* L. (eelgrass). J Exp Mar Biol Ecol 130:93-109

6 Acknowledgements

This project was funded by the Western Australia Marine Science Institution (WAMSI) as part of the WAMSI Kimberley Marine Research Program (Project 2.2.3), and an Australian Research Council (ARC) Future Fellowship grant (FT110100201) to RJL. Additional support was provided by the ARC Centre of Excellence for Coral Reef Studies (CE140100020). We are grateful for the field assistance and guidance provided by the Bardi Jawi Rangers in One Arm Point, as well as the Bardi Jawi people through their advice and consent to access their traditional lands. Thanks also to the Kimberley Marine Research Station for their support of the field logistics. Mike Cuttler, Jordan Iles, Miela Kolomaznik, Leonardo Ruiz Montoya, and Nick Mortimer provided invaluable field assistance.

7 Communication

7.1 Students supported

- Renee Gruber, The University of Western Australia, PhD, expected completion December 2016, "Productivity and biogeochemical processes on a macrotidal tropical reef platform".

7.2 Journal publications

- Lowe, R., Pivan, X., Symonds, G., Falter, J., Gruber, R. (2016) Rising sea levels will reduce extreme temperature variations in tide-dominated reef habitats, Science Advances, e1600825.
- Lowe, R., Falter, J. (2015) Oceanic forcing of coral reefs, Annual Review of Marine Science, 7: 43-66
- Dandan, S., Falter, J., Lowe, R., McCulloch, M. (2015) Resilience of coral calcification to extreme

temperature variations in the Kimberley region, northwest Australia, Coral Reefs, 34 (4): 1151-1163

7.3 Submitted manuscripts

- Gruber, R., Lowe, R., Falter, J. (2016) Metabolism of a tide-dominated reef platform with extreme diel temperature and oxygen variations, Limnology and Oceanography, *in revision*.

7.4 Presentations

- Gruber, R.K., Lowe, R.J., and Falter, J.F. Community production and respiration in an extreme environment: New insights from tropical tide-dominated fringing reefs. International Coral Reef Symposium. Honolulu, Hawaii, USA. June 2016.
- Lowe, R.J. Benthic community productivity of the Kimberley's macrotidal reefs", DPaW Lunch and Learn seminar, April 2016.
- Lowe, R.J. Exploring the circulation and heat balances of northwestern Australia's remote macrotidal reefs, ARC Centre of Excellence for Coral Reef Studies Symposium, Hobart, October 2015.
- Lowe, R.J. Environmental forcing of benthic community productivity within the Kimberley's macrotidal reefs, WAMSI Research Conference, March 2015.
- Lowe, R.J. Oceanic drivers of coral reef systems along Western Australia, ARC Centre of Excellence for Coral Reef Studies Symposium, Canberra, October 2014.
- Lowe, R., Gruber, R.K., Falter, J. Hydrodynamics of the macrotidal reef systems in northwestern Australia, ALSO/AGU Ocean Sciences Meeting, Honolulu, Hawaii, USA. February 2014.
- Gruber, R.K., Lowe, R., Falter, J. Linkages between productivity, nutrient uptake, and allochthonous nutrient inputs on tropical macrotidal fringing reefs. ALSO/AGU Ocean Sciences Meeting. Honolulu, Hawaii, USA. February 2014.

7.5 Other communications achievements

- Lowe, R.J. "Kimberley tides and ocean circulation", Science on the Broome Coast – Public Talk, August 2016
- Gruber, R.K., R.J. Lowe. "Pushing the frontiers of reef research." *Kimberley Science and Conservation News*. June 2014: pg 4. WA Dept. of Parks and Wildlife (Web).
- Gruber, R.K. and R. J. Lowe. 2014 Pushing the frontiers of reef research. Landscope 30 (1): 42-43.
- Gruber, R.K. and R. J. Lowe. "Benthic productivity – fieldwork findings." Presentation to Bardi Jawi Rangers at conclusion of fieldwork, One Arm Point, WA. April 2014.
- Gruber, R.K., R.J. Lowe, and N. Cayabyab. "Benthic productivity on a fringing reef." Presentation to Cygnet Bay community, Cygnet Bay Pearl Farm, WA. October 2013.